Phenotypic diversity and sensitivity to injury of the pulmonary endothelium during a period of rapid postnatal growth

Fabio Zanini[1], Xibing Che[2,3], Carsten Knutsen[2,4], Min Liu[2,4], Nina Suresh[2,3], Racquel Domingo-Gonzalez[2,4], Steve H. Dou[2,4], Robert C. Jones[5], David N. Cornfield[2,3,*], Stephen R. Quake[5,6,7,*], and Cristina M. Alvira[2,4,*]

*: these authors contributed equally

[1]Prince of Wales Clinical School, Lowy Cancer Research Centre, University of New South Wales, Sydney, Australia

[2]Center for Excellence in Pulmonary Biology, Stanford University School of Medicine, Stanford, CA

[3]Division of Pulmonary, Asthma and Sleep Medicine, Department of Pediatrics, Stanford University School of Medicine, Stanford, CA

[4]Division of Critical Care Medicine, Department of Pediatrics, Stanford University School of Medicine, Stanford, CA

[5]Department of Bioengineering, Stanford University, Stanford, CA

[6]Chan Zuckerberg Biohub, San Francisco, CA

[7]Department of Applied Physics, Stanford University, Stanford, CA

Address for Correspondence:

Cristina M. Alvira, M.D.
Stanford University School of Medicine
Center for Excellence in Pulmonary Biology
770 Welch Road, Suite 435
Palo Alto, CA 94304
Tel: 650-723-7297, FAX: 650-725-0171
Email: calvira@stanford.edu

Abstract:

Background: Endothelial cells (EC) sit at the forefront of dramatic physiologic changes occurring in the pulmonary circulation during late embryonic and early postnatal life. First, as the lung moves from the hypoxic fetal environment to oxygen-rich postnatal environment, marked changes in pulmonary EC structure and function facilitate a marked increase in blood flow from the placenta to the lungs. Subsequently, pulmonary angiogenesis expands the microvasculature to drive exponential distal lung growth during early postnatal life. Yet, how these marked physiologic changes alter distinct EC subtypes to facilitate the transition of the pulmonary circulation and regulate vascular growth and remodeling remains incompletely understood. **Methods:** In this report, we employed single cell RNA-transcriptomics and in situ RNA imaging to profile pulmonary EC in the developing mouse lung from just before birth through this period of rapid postnatal growth. **Results:** Multiple, transcriptionally distinct macro- and microvascular EC were identified in the late embryonic and early postnatal lung, with gene expression profiles distinct from their adult EC counterparts. A novel arterial subtype, unique to the developing lung localized to the distal parenchyma and expressed genes that regulate vascular growth and patterning. Birth particularly heightened microvascular diversity, inducing dramatic shifts in the transcriptome of distinct microvascular subtypes in pathways related to proliferation, migration and antigen presentation. Two distinct waves of EC proliferation were identified, including one just prior to birth, and a second during early alveolarization, a time of exponential pulmonary angiogenesis. Chronic hyperoxia, an injury that impairs parenchymal and vascular growth, induced a common gene signature among all pulmonary EC, unique alterations to distinct microvascular EC subtypes, and disrupted EC-EC and EC-immune cell cross talk. **Conclusions:** Taken together, these data reveal tremendous diversity of pulmonary EC during a critical window of postnatal vascular

growth, and provide a detailed molecular map that can be used to inform both normal vascular development and alterations in EC diversity upon injury. These data have important implications for lung diseases marked by dysregulated angiogenesis and pathologic pulmonary vascular remodeling.

Introduction:

At birth, rhythmic distention of the lungs and a marked rise in oxygenation rapidly decrease pulmonary vascular resistance to increase pulmonary blood flow. Lining the pulmonary blood vessels, endothelial cells (EC) serve as first responders to these dramatic changes in oxygen and shear stress by increasing the production of endothelial-derived vasodilators and altering their cell shape to facilitate successful transition of the fetal to neonatal circulation[1]. Subsequently, rapid expansion of the pulmonary microcirculation during early postnatal life drives the formation of hundreds of millions of alveoli to dramatically increase gas exchange surface area.[2-4]

Completion of parenchymal and vascular development after birth renders the immature, neonatal lung highly susceptible to environmental insults that can disrupt development. This is frequently observed in the context of preterm birth, where disrupted pulmonary angiogenesis and alveolarization results in the chronic lung disease, bronchopulmonary dysplasia (BPD), the most common complication of prematurity[5]. Moreover, even in the mature lung, developmental mechanisms and gene expression programs are reactivated to promote lung regeneration after injury[6,7 8 9]. Thus, a detailed understanding of pulmonary EC diversity and phenotypic changes across postnatal development has important implications for lung diseases affecting not only premature infants, but also older infants, children, and adults.

EC are highly heterogeneous, often displaying multiple phenotypes even within a single organ, and tremendous plasticity in response to changes in the microenvironment. However, current knowledge about the molecular regulation of pulmonary angiogenesis is largely based upon studies performed on whole lung, which is limited by ensemble averaging, or extensively passaged primary cells. Single cell transcriptomics has provided a high-resolution picture of the adult lung in mice[10] and humans[11] and begun to shed light on specific populations in the epithelial[12]

and immune compartments[13, 14]. However, the distinct EC subtypes composing the immature lung vasculature and their spatial locations, and physiological roles have not been fully characterized. In this study we utilized single cell RNA-sequencing (scRNASeq) and *in situ* hybridization to elucidate discrete EC subtypes and identify developmental alterations in the EC transcriptome during early postnatal life and assess how EC diversity and phenotype is altered by injuries that disrupt lung parenchymal and vascular growth.

Results:

Pulmonary endothelial heterogeneity increases after birth

To obtain a high-level description of perinatal endothelial heterogeneity in the lung, we isolated lungs from single male and female C57BL/6 mice at E18.5 (early saccular), P1 (late saccular), P7 (early alveolarization) and P21 (late alveolarization), and single male and female P7 mice exposed to chronic hyperoxia, an injury that impairs alveolarization and angiogenesis (Fig. 1A). After optimizing lung dissociation to maximize EC viability and yield[14], we perfused the pulmonary circulation, digested the lungs and performed fluorescent activated cell sorting (FACS) to select CD31+ EC. We transcriptionally profiled 2931 EC from 10 C57BL/6 mouse lungs using plate-based scRNASeq, at a depth of approximately 1 million reads per cell.[15] We visualized the data with Uniform Manifold Approximation and Projection (UMAP)[16], and performed unsupervised clustering using the Leiden algorithm[17] to reveal nine transcriptionally distinct EC subtypes in the developing perinatal lung (Fig.1B). These included four groups of macrovascular EC (including two distinct arterial clusters), proliferative EC, and four microvascular EC (MEC) clusters broadly distinguished from one another by developmental timepoint and expression of the gene carbonic anhydrase 4 (*Car4*) (Fig. 1C). Visualization of

individual cells by developmental stage revealed a dramatic shift in the endothelial landscape after birth, with the disappearance of embryonic MEC, and the appearance of the three postnatal MEC clusters (Fig. 1D). This developmental shift was accompanied by significant gene expression changes, including genes primarily expressed prior to birth (e.g. *Ankrd37* and *Depp1*) (Fig. 1E), and other genes expressed only after birth (e.g. *Pde3a* and *Hpgd*) (Fig. 1F).

Pulmonary EC in the perinatal lung are transcriptionally distinct from the adult.

We next determined how similar our EC subtypes are to adult lung EC by directly comparing our data with the single cell mouse atlas, Tabula Muris (TM)[10] (Fig. 2A), containing data from 3-month old mice. Harmonization of the two data sets highlighted the marked difference between immature lung EC compared to their mature counterparts, particularly within the microvasculature. Our lymphatic EC embedded close to the TM lymphatic EC, suggesting a similar phenotype (Fig. 2B). Our arterial EC also embedded close to the TM arterial cluster, with our arterial II EC appearing more similar to adult lung arterial EC. Interestingly, our venous EC were quite far from adult venous EC, suggesting significant alterations in phenotype during postnatal development. Our *Car4*+ MEC also embedded close to the TM *Car4*+ MEC, but a developmental gradient was evident with our P21 *Car4*+ MEC embedding closest to the adult, and P1 farthest away (Fig. 2C). Proliferative EC were an entirely unique cluster in our data set, confirming the absence of proliferation in the healthy adult pulmonary endothelium. The *Car4*- MEC formed adjacent clusters that layered developmentally, with the embryonic EC at the top, followed by the early *Car4*- MEC, followed by the late *Car4*- MEC, which embedded closest to the TM adult *Car4*- MEC (Fig 2B and C). Taken together, these data highlight the marked heterogeneity of the developing lung EC, and demonstrate that the majority of EC subtypes in the

developing lung are transcriptionally distinct from, and slowly converge over time towards their adult counterparts.

Two transcriptionally distinct arterial subtypes are present in the perinatal lung

We first clarified the transcriptional profiles of macrovascular EC. Lymphatic EC (cluster 4) demonstrated exclusive expression of characteristic lymphatic genes *Thy1*[18] and *Prox1*[19], and *Ccl21a,* a chemokine that selectively stimulates T lymphocyte chemotaxis[20] (Fig. 3A). Similarly, venous EC (cluster 3) shared expression of *Vwf* with arterial EC, but was distinguished by the expression of *Nr2f2*[21] (data not shown), a transcription factor that suppresses Notch signaling to confer venous identity[22] (Fig. 3B). Venous EC also uniquely expressed high levels of *Car8* and *Mmp2*, genes not previously reported as specific venous markers. Arterial cells shared expression of *Gja5*[23], a gene that modulates arterial identity[23] and *Bmx*, a tyrosine kinase expressed in large arteries[24] (Fig. 3C), but were split by the clustering algorithm into two subtypes, arterial I (cluster1) and arterial II (cluster 2). The arterial II subset was distinguished from arterial I by the high expression of *Kcne3*, encoding a potassium channel subunit selectively expressed by tip cells and the developing vasculature[25], and *Dkk2,* an inhibitor of canonical Wnt signaling[26]. Quantification of these four macrovascular EC subtypes across perinatal development highlighted a gradual increase in venous EC abundance, and a marked decrease in arterial I EC abundance between P7 and P21 (Fig. 3D).

The disappearance of arterial I EC by P21, combined with prior reports identifying a single arterial cluster in the adult lung, suggested that arterial I are a transcriptionally distinct pulmonary arterial EC unique to the developing lung. We localized arterial EC I and II *in situ* by simultaneously detecting *Cdh5*, *Gja5*, and *Dkk2* mRNA, and identified arterial cells lining small

arterioles as exclusively arterial II, characterized by co-expression of *Gja5* and *Dkk2*. In contrast, arterial I EC expressing *Gja5* but not *Dkk2* were located in the distal lung parenchymal, adjacent to *Gja5*$^{-}$*Cdh5*$^{+}$ microvascular EC (Fig. 3E).

Differentially expressed genes in arterial I and II EC were enriched for distinct pathways related to vascular growth and remodeling (Fig. 3F and G and Supplemental Table 1). In arterial I EC, the highest enrichment was found in "vascular development", including high expression of *Col4a1* and *Col4a2*, integral components of the vascular basement membrane[27], and angiogenic genes such as *Ets1*[28, 29], *Robo4*[30], *Foxf1*[31] and *Kit*[32]. Additional up-regulated genes included *Rasgrp3*, a guanine exchange factor expressed in embryonic and nascent vessels[33], and *Igfbp7*, encoding a secreted angiocrine factor[34] also expressed in nascent vasculature, thought to regulate vascular patterning by serving as an ECM binding protein to prevent excessive VEGF-A bioavailability[35]. "Extracellular matrix organization" and "elastin fiber assembly" were enriched in arterial II EC, including high expression of *Bgn*, an ECM component that enhances HIF-1α-mediated transcription of VEGF[36], and multiple genes important for elastin assembly including *Eln*, *Lox,* and *Fbln2*[37]. Response to growth factor and cell-substrate adhesion were additional enriched pathways, including high expression of the Notch ligand *Jag1*, that promotes maturation of newly formed vessels[38], *Cldn5*, encoding a tight junction protein that promotes EC barrier function[39], and *Ltbp4,* a TGFβ binding protein required for normal alveolar septation[40].

Although the abundance of the arterial II EC was relatively stable during postnatal lung development, gene expression within this cluster changed across time. The angiogenic inhibitor *Serpinf1*, important for vascular pruning[41], was expressed through P7, but no longer expressed by P21. Similarly, expression of the pro-angiogenic gene *Dkk2*[42] exhibited a more gradual decrease over development. Conversely, expression of *Ctsh*, a cysteine cathepsin with a recently described

pro-angiogenic function[43] increased over time. Taken together, these data suggest relatively stable venous and lymphatic EC, but dynamic alterations in the abundance and gene expression programs of arterial I and II cells, providing a fine-tuned regulation of vascular growth and patterning during early postnatal life along both canonical and non-canonical pathways.

Pulmonary microvascular EC diversity increases during early postnatal life

We then focused our attention on the four transcriptionally distinct microvascular (MEC) populations, three of which were associated with specific timepoints. First, embryonic MEC (cluster 6) was almost exclusively populated by EC obtained from E18.5 (Fig. 1D). Embryonic MEC represented almost 60% of total EC just prior to birth, and were distinguished from postnatal MEC (Clusters 7-9) by the expression of *Depp1*, a hypoxia-induced gene that regulates FOXO3-mediated autophagy[44, 45], *Sparcl1*, a gene that promotes EC quiescence and vascular stability by enhancing mural cell recruitment[46], and the HIF-1α target *Rgcc,* a complement response gene that promotes placental angiogenesis by enhancing NFκB-mediated VEGFR2 expression[47] (Figure 4A). The embryonic MEC also expressed high levels of *Mest*, a paternally imprinted gene with a putative role in angiogenesis[48, 49], *Gas5*, a long non-coding RNA that promotes stemness and prevents EC senescence[50-52], and *Npm1*, a gene that promotes embryonic stem cell proliferation[53].

Embryonic MEC abundance dropped dramatically after birth (Fig. 4B), replaced at P1 to P7 by increasing abundance of two postnatal MEC clusters. While *Car4*+ MEC were present at all postnatal timepoints (see below), early *Car4*- MEC (cluster 7) consisted almost exclusively of EC from P1 and P7 (Fig. 4C). This subtype itself was eventually replaced by late *Car4*- MEC (cluster 8) almost exclusively comprised of EC from P21. We performed RNA velocity[54] on both *Car4*- MEC subtypes and reconstructed a cellular trajectory from early *Car4*- to late *Car4*– MEC along

the embedding, with a general downwards flow, suggestive of continuous progression (Fig. 4C). Taken together these data suggest that these two transcriptional clusters represent different developmental states of the same cell type rather than distinct cell types.

We next explored genes that were differentially expressed between early and late *Car4*- MEC. One of the most highly expressed genes by early *Car4*- MEC was the paternally expressed gene-3 (*Peg3*), an imprinted gene that encodes a zinc finger protein highly expressed during embryogenesis[55, 56] that marks cells capable of self-renewal in adult tissues[57] (Fig. 4D). We employed *in situ* hybridization to detect *Peg3* expression in MEC from mice at P7 and P21. In agreement with our computational data, *Peg3*+ EC were abundant throughout the distal pulmonary endothelium at P7. In contrast, *Peg3*+ EC were rare in the P21 lung, with 3-fold greater *Peg3*+ EC in P7 compared to P21 lungs. Pathway analysis of genes up-regulated in early *Car4*- MEC identified enrichment in pathways regulating actin cytoskeletal organization including high expression of *Cotl1*, a gene that promotes lamellipodia protrusion[58], and multiple genes that regulate cell motility including *Fscn1*, *Twf1*, *Twf2*, *Cd81* and *Nrep* (Fig. 4F and Supplemental Fig. 1). Genes that promote proliferation were also increased including *Peg3, Ccnd1*, *Ccnd3, and Csrp2*, as were multiple angiogenic genes including *Rara*, the gene encoding the retinoic acid receptor alpha[59], *Adam15,* a metalloproteinase that promotes EC survival[60] and retinal neovascularization[61], and *Cd40*, a cell surface receptor that enhances VEGF expression[62]. Late *Car4*- MEC were characterized by a general down-regulation of these genes, in concert with a significant up-regulation of *Cd36*, a receptor for thrombospondin that inhibits EC migration[63], *Itga1*, a component of the α1β1 integrin that binds the basement membrane components collagen IV and laminin with high affinity[64], and *S1pr1*, encoding a G-protein coupled receptor for syphingosine-1-phosphate that enhances EC barrier function and stability of nascent vessels[65, 66].

Car4+ MEC exhibit dynamic changes in gene expression to influence cell migration, angiogenesis and immunity.

The second MEC subtype that emerged at birth were *Car4+* MEC (cluster 9), in agreement with recent reports, a specialized MEC that require alveolar epithelial type I-derived VEGF for survival[67], and appear to play a key role in both alveolarization and lung repair after viral infection[68]. However, the specific functions of *Car4+* MEC during lung development are not known. In addition to high expression of *Car4*, these cells were distinguished from other EC by increased expression of *Fibin*, a gene downstream of retinoic acid and Wnt signaling pathways[69], the transcriptional repressor *Tbx2*, and *Sirpa*, encoding a cell surface receptor for CD47 (Fig. 5A). Localization of the *Car4+* MEC by detecting simultaneous expression of *Car4*, *Tbx2*, and *Cdh5* confirmed the presence of *Car4+* MEC in the distal lung, interspersed with *Car4-* MEC as has been recently described [67](Fig. 5B). A number of transcription factors (TFs) were positively correlated with *Tbx2* expression (Fig. 5C) including *Tbx3,* a TF required for development of the cardiac outflow tract [70] and kidney vasculature[71], *Prdm1*, a TF downstream from VEGFR2 that serves to maintain tolerance in neonatal intestinal cells[72], and *Hopx*, a TF that integrates Bmp and Wnt signaling[73]. Conversely, TFs down-regulated in *Car4+* MEC included *Hoxa5*, a repressor of VEGFR2 that maintains EC quiescence[74], *Foxo1,* important for embryonic and yolk sac vascularization[75], and *Hey1,* a downstream effector of Notch[76].

Although *Car4+* MEC contained EC derived from all three postnatal timepoints, a clear developmental gradient was apparent. Pseudotime analysis and RNA velocity confirmed this general trend (Fig. 5D). Identification of select genes exhibiting varied expression over pseudotime demonstrated a weak pattern of highly expressed genes slowly increasing, and a more dramatic

decrease in many genes (Fig. 5E). Pathway analysis of DEGs at each developmental timepoint (Fig. 5F-I) and the expression of select genes across pseudotime (Fig. 5J) revealed that *Car4+* MEC at P1 expressed genes important for cell migration and cytoskeletal remodeling, including *Adam10*, a metalloproteinase that promotes EC permeability by degrading VE-Cadherin[77], and *Itga2* and *Itga4*, components of the integrin receptors for collagen and fibronectin. By P7, genes related to vascular development were upregulated, including *Eng*, an ancillary TGFβ receptor essential for extraembryonic angiogenesis[78], *Tspan12*, a tetraspanin that regulates retinal vascular development by augmenting Norrin signaling[79], and *Ywhaz,* encoding a 14-3-3 adapter protein required for lung vascular development[80]. By P21 these, and other genes important for blood vessel morphogenesis were down-regulated, including *Egfl7*, a ligand for αvβ3 integrins that promotes EC migration[81], and *Jcad*, an EC junctional protein that suppresses Hippo signaling[82]. Enriched pathways in the P21 *Car4+* MEC included antigen processing and presentation, including up-regulation of *Cd36,* an endocytic scavenger receptor involved in the presentation of MHC class II antigens[83], and *H2-D1* and *H2-K1*, genes encoding MHC Class I molecules. Of note, at the most advanced pseudotime, gene expression was generally markedly decreased across all pathways, similar to the pattern observed in the late *Car4-* MEC, consistent with a global switch across MEC toward a quiescent phenotype at later development.

Proliferating EC peak just prior to birth and again during early alveolarization

Proliferating EC (cluster 5) were distinguished by high expression of *Mki67*, and additional genes associated with proliferation and cell cycle regulation, including *Hmmr*[84] and *Neil3*[85] (Fig. 6A). Quantification of proliferating EC revealed two distinct waves of proliferation. The first occurred just prior to birth, with proliferative EC comprising almost 40% of total EC at E18.5.

After birth, EC proliferation decreased dramatically, but increased again at P7 prior to virtual disappearance of proliferating EC by P21(Fig. 6B). Localization of proliferating EC in the P7 lung allowed differentiation of proliferating EC in from non-proliferating EC, with proliferating EC frequently located in spatial clusters (arrow). Of note, many of the proliferative EC (Cluster 5) also expressed *Peg3* (Fig. 4E), but little *Car4*+ (Fig 5A), suggesting that postnatal proliferative EC were more closely related to the early *Car4*- MEC population.

We next explored the transcriptional programs driving EC proliferation at these key timepoints. We compared TF expression in non-proliferative versus proliferative EC, and identified the Myb and E2F families as TF families with the greatest enrichment among up-regulated genes in proliferating EC compared to all TFs in the genome (Fig. 6D). To determine the likelihood of this enrichment occurring by chance, we ran simulations of randomly chosen TFs and compared the fold-enrichment occurring by chance with the observed enrichment in our dataset. For both families, the observed enrichment was greater than any random enrichment (Fig. 6E), in contrast to other TF families (e.g. MH1), where the enrichment occurring by chance in some simulations achieved or surpassed the observed enrichment (Supplemental Figure 2). We then identified specific members within these two families that were shared or unique between proliferating EC at E18.5 and P7. Although many of the up-regulated TFs were shared, *Mybl2* enrichment was 3.75-fold greater in proliferating EC at P7 than at E18.5 (Fig. 6F and G). To determine the functional significance of *Mybl2* in microvascular EC at P7, we silenced *Mybl2* in primary lung microvascular EC isolated from mice at P7, and found that loss of *Mybl2* significantly blunted EC proliferation in response to endothelial growth media (Fig. 6H), and impaired survival, as evidenced by an increase in active caspase-3 immunostaining (Fig. 6I).

Chronic hyperoxia disrupts the transcriptome of specific endothelial subsets and delays microvascular maturation.

After obtaining a high-resolution picture of perinatal lung EC from health animals, we then performed single cell transcriptomics on pulmonary EC isolated from P7 pups exposed to chronic hyperoxia (Fig. 1A), an established model that recapitulates the arrested lung and vascular development observed in premature infants with BPD. We compared EC derived from normoxic and hyperoxic mice at P7 and found alterations in both relative abundance and gene expression within select subtypes. Dimensionality reduction via UMAP for EC from P7 only revealed well mixed macrovascular EC but greater segregation within MEC (Figure 7A and B). Embryonic MEC, which were restricted to earlier time points in normoxic mice, persisted at P7 in hyperoxic mice, and late *Car4*- MEC were less abundant (Figure 7C), consistent with the arrested lung development observed in infants with BPD. Further, a novel cluster of proliferating venous EC was present, comprised almost exclusively by EC from hyperoxic lungs.

Despite the vast transcriptional heterogeneity of lung EC in health P7 mice, hyperoxia induced a common gene signature across all EC subtypes (Figure 7D). Commonly up-regulated genes included *Cdkn1a*, an inhibitor of cell proliferation[86] that also limits oxidative stress[87], *Eda2r*, a member of the TNF receptor superfamily that is increased in the aging lung[88], and the p53 down-stream target genes, *Zmat3,* an inhibitor of cell growth[89], and *Phlda3*, a repressor of Akt signaling[90]. Commonly down-regulated genes in hyperoxia included microRNA (miR) miR6236, a miR with unclear significance in EC, but predicted targets that include *Foxc2*, *Myl6b*, *Pdgfa*, and *Adgrl3*. Additional common down-regulated genes included *Sox7*, a member of the SRY-related HMG-box family of TFs that promotes endothelial fate and arterial specification[91, 92], *Pfkb3*, a

gene important in fructose metabolism that promotes angiogenesis[93], and *Klhl2*, a regulator of WNK kinases[94].

In addition to this common response, hyperoxia also induced profound and distinct transcriptomic alterations in select EC subtypes, including the *Car4*- and *Car4*+ MEC and the proliferative EC (Fig. 7F). In early *Car4*- MEC, hyperoxia suppressed numerous genes that regulate EC homeostasis and angiogenesis (Fig. 7F and Supplemental Table 2). One of the most down-regulated genes was *Ntrk2*, encoding a neurotrophin receptor that promotes Ets-1 mediated transcription of *Cdh5*[95], neovascularization[96], EC migration[97], and vascular relaxation[98]. Hyperoxia also suppressed additional angiogenic genes in *Car4*- MEC including *Sparcl1*, *Glul, a* gene that promotes angiogenesis via a mechanism distinct from glutamine synthesis[99], *Ets1,* a TF required for EC survival during embryonic angiogenesis[29], and *Wfdc1*, a factor that enhances EC migration and pericyte recruitment[100], and down-regulated MCH class I genes including *H2-Q7*, *H2-K1*, and *H2-D1*. Up-regulated genes included *Lyve1*, a hyaluronan receptor highly expressed by lymphatic EC that promotes dendritic cell trafficking[101], *Serpine2,* a potent thrombin inhibitor[102], and the vasoconstrictor *Edn1*. Of note, hyperoxia also increased the expression of *Apln* and *Mmrn2* in the *Car4*- MEC, two genes primarily expressed by *Car4*+ MEC in the normoxic lung.

Hyperoxia dysregulated similar pathways, but distinct genes, in proliferative EC (Fig. 7F and Supplemental Table 3). Similar to the early *Car4*- MEC, hyperoxia suppressed the expression of MHC class I genes. Further, both *Kit* and *Aplnr*, receptors for pathways that promote EC proliferation were specifically suppressed by hyperoxia. Expression of *Fhl1*, a gene that can either promote or inhibit cell proliferation, was also significantly down-regulated[103]. Up-regulated genes included *Bax* a gene promoting apoptosis, *Btg2*, a gene that inhibits proliferation, *Gdf15*, a

cytokine up-regulated with oxidative stress, *Gtse1*, a gene involved in p53-mediated cell cycle arrest, and *Terf1*, a telomere binding protein that negatively regulates telomere length. Taken together, these data suggest a number of mechanisms that may contribute to the impaired vascular growth observed in response to hyperoxia.

Hyperoxia also induced unique alterations to the *Car4*+ MEC transcriptome (Fig. 7F and Supplemental Table 4). Top genes suppressed by hyperoxia included *Cav2*, encoding a protein that prevents lung hypercellularity and abnormal EC proliferation[104], the oxidative stress mediator, *Txnip*[105], *Dpp4*, an extracellular peptidase that regulates chemokine and growth factor activity[106], *Mapt,* a regulator of endothelial barrier function[107], and *Hpgd,* important for prostaglandin PGE2 metabolism. Up-regulated genes included *Cd63,* a transmembrane glycoprotein that enhances VEGFR2 downstream signaling[108], potentially representing a compensatory response given the dependence of *Car4*+ MEC on epithelial-derived VEGF for survival[67]. Additional up-regulated genes included genes that inhibit NFκB activation (e.g. *Nrros*[109] and *Tspan6*[110]), a pathway essential for postnatal pulmonary angiogenesis[111], and a marked increase in *Inhba,* encoding a TGF-β family member that impairs VEGF-mediated EC angiogenesis and proliferation[112].

We validated the dysregulated expression of select genes by multiplex *in situ* hybridization. In normoxic P7 lungs, numerous MEC in the distal lung exhibited intense staining for *Ntkr2* (Fig. 7G), in contrast to virtually absent endothelial *Ntrk2* staining in the hyperoxic lung. In contrast, in normoxic lungs, *Inhba* expression was minimal (Fig. 7H), but markedly increased by hyperoxia, with numerous *Car4*+ MEC specifically exhibiting high expression of *Inhba* (arrows).

Alterations in cell communication within endothelial subtypes and between EC and immune cells during development and in response to injury.

Given the heterogeneity within the neonatal lung endothelium (Figure 1B), we asked how different EC subtypes communicate with one another across development, and how this communication is altered by hyperoxia. First, we identified the number of specific, potential ligand-receptor interactions between each EC subtype at each timepoint (Figure 8A). We observed the largest number of interactions at early postnatal time points, with interactions in MECs and venous EC peaking at P1, and interactions in lymphatic and arterial EC peaking at P7. The latter two macrovascular populations also participated in the largest number of EC-EC interactions at all time points except P21. We then stratified the data by both emitting and receiving cell subtype (Figure 8B). Among all populations and times, lymphatic EC at P7 had the highest number of interactions with themselves and with arterial EC. Interestingly, a gradient from macrovascular to microvascular EC was observed in these heatmaps, with the arterial EC I cells located in the middle, consistent with an intermediate phenotype. At P21, venous EC retained more interactions than other subtypes, particularly with themselves and with *Car4*+ MEC, and the global landscape lacked the gradient observed at P7. Hyperoxia flattened this interaction table (Figure 8C), inducing a loss of interactions in lymphatic and arterial EC (downward triangles), and an increase in interactions between MECs (upward triangles).

Hyperoxia also appeared to dysregulate cross-talk between the *Car4*+ and *Car4*- MEC. In normoxia, *Car4*+ EC highly expressed *Apln*, a gene promoting EC proliferation and angiogenesis[86], and *Car4*- MECs highly expressed the receptor *Aplnr* (Figure 8D, top). Hyperoxia markedly decreased *Aplnr* in *Car4*- MEC but increased *Apln* expression in *Car4*+ MEC, suggesting a potential compensatory response. In normoxia, expression of *Kitl*, the gene encoding stem cell factor, was highest in *Car4*+ MEC, while the receptor, *Kit* (expressed in putative EC progenitors with a key role in alveolarization[30, 87]), was highly expressed by *Car4*- MEC (Figure

8D, bottom). Hyperoxia significantly down-regulated both *Kitl* and *Kit* in their respective populations. Taken together, these data suggest that hyperoxia significantly compromises key pathways that promote EC proliferation and vascular growth.

As cells lining the blood vessels, EC are also positioned to interact with circulating immune cells. We therefore examined the interactions between EC and immune cells in the developing lung[14]. At E18.5, putative endothelial-immune cell communication was highest between basophils and multiple EC subtypes, including arterial and proliferating EC (Figure 8E), with embryonic basophils and mast cells expressing ligands for VEGF and FGF signaling pathways (Supplemental Table 5). Similarly, Mac I cells, a unique embryonic macrophage that encircles small arterioles expressed VEGF pathway ligands (e.g. *Vegfb* and *Pgf*), and *Fn1*, an ECM protein essential for blood vessel morphogenesis[113] (Supplemental Tables 6 and 7). Moreover, the interaction between endothelial and immune cells may be facilitated by selective expression of *Cxcl12* (Figure 8G), a chemokine that promotes chemotaxis of *Cxcr4* expressing cell populations[114], expressed by both the arterial EC and *Car4*- MEC (Figure 8F). At E18.5, basophils were the immune population expressing the highest levels of *Cxcr4*. A secondary receptor for *Cxcl12*, *Ackr3*, which lacks an intracellular signaling domain, was expressed at high levels by venous EC. These data suggest that *Cxcl12-Cxcr4* signaling is high in the pre-capillary vasculature, facilitating immune cell extravasation from the blood to the tissue. This signaling diminishes from the arteries to the capillaries, and upon reaching the post-capillary vasculature, is replaced by *Cxcl12-Ackr3* signaling, perhaps serving to clear residual *Cxcl12* and prevent unwanted immune cell extravasation downstream of pulmonary veins.

Globally, postnatal interactions between macrophages and macrovascular EC predominated, with putative interactions between Mac IV cells (macrophages found adjacent to

blood vessels[14]) persisting between venous EC and MEC at P21, a time when other putative interactions were decreasing. Hyperoxia heightened the number of interactions between Mac IV cells and select EC subtypes including the arterial I EC, venous EC, proliferative EC, and *Car4*-MEC.

Discussion

As the lungs transition from a liquid-filled, relatively hypoxic environment *in utero* to oxygen-rich air-breathing life, the pulmonary vasculature undergoes dramatic changes to permit sufficient blood flow to the lungs to supply oxygen to the body. Subsequently, exponential growth of the microvasculature during early postnatal life drives alveolarization, markedly increasing gas exchange surface area. In this study, we employed single cell transcriptomics, mechanistic studies in primary EC, and *in situ* hybridization to identify alterations in endothelial heterogeneity occurring during this discrete period of vascular growth and remodeling, and define the effect of hyperoxia on the transcriptomic ontogeny of the pulmonary endothelium.

In this study we identified a number of key findings. Although all macrovascular EC subtypes were present in the late embryonic lung, microvascular EC heterogeneity increased upon birth with the separation of non-proliferative embryonic MEC into three distinct subtypes distinguished by timepoint and the expression of *Car4*[67]. Moreover, *Car4*+ MEC were entirely absent at E18.5 but relatively abundant at P1, indicating a rapid and robust emergence of this transcriptionally distinct subtype from preexisting precursors after birth. Harmonization of our data with single cell transcriptomic data from the adult mouse lung demonstrated that although there was broad agreement with EC subtypes, the transcriptome of immature lung EC were entirely different from mature lung EC, particularly with respect to the MEC. Proliferating EC,

completely absent in the adult lung, peaked in two separate waves during late lung development, one just prior to birth and a second wave during early alveolarization, a period of rapid angiogenic growth. Hyperoxia induced diverse and profound alterations including: i) gene expression changes common in all EC subtypes; ii) unique transcriptional dysregulation in select MEC; and iii) disrupted EC-EC and EC-immune cell communication. Taken together, these data highlight the continued evolution of lung EC phenotype during early postnatal development, and the sensitivity of the immature pulmonary endothelium to injury.

An additional important finding of our study was the presence of a unique, but transient subtype of arterial EC that has not been previously identified. These arterial I EC peaked at E18.5 and disappeared by P21, a time when angiogenesis is slowing and the vasculature is moving toward quiescence. In contrast to the arterial II EC which localized to larger arteries and small arterioles, arterial I EC localized to the distal lung, adjacent to *Car4*- MEC. Consistent with this finding, arterial I EC were assigned between arterial II EC and *Car4*- MEC by the harmonized UMAP embedding containing the neonatal and adult data, suggesting that arterial EC II are a more mature subtype, while the arterial I EC are phenotypically closer to MEC. In depth analysis of the transcriptional differences between the two identified vascular development as the most enriched pathway in arterial I EC, including the up-regulation of numerous genes expressed by nascent blood vessels that regulate vascular growth and patterning. Future studies at timepoints between P7 and P21, and methodologies such as *Gja4* lineage tracing will be necessary to establish whether arterial I EC gradually transition into either arterial EC II or early *Car4*- MEC, and to define the physiological function of this developmentally-specific arterial EC.

Among the microvascular EC, *Car4*- MECs spanned three transcriptionally distinct clusters: the non-proliferative embryonic MEC, early *Car4*- MEC, and late *Car4*- MEC, each

peaking at distinct timepoints. This developmental diversity challenges recent descriptions of the *Car4*- lung MEC as a static 'general' capillary that resembles capillaries in other organs[115]. Analysis of the differentially expressed genes between the early and late *Car4*- MEC suggested that early *Car4*- MEC exhibit greater proliferative and migratory potential than their late counterparts. This is consistent with our previous observation that primary MEC isolated from the early alveolar lung proliferate and migrate more quickly than those isolated from the adult lung[111]. One of the most highly up-regulated genes in early *Car4*- MEC was *Peg3*, a paternally imprinted gene that marks specific progenitor populations capable of self-renewal in adult tissues[57]. *Peg3*+ EC are abundant in the embryonic but rare in the adult vasculature, and appear to represent EC with high proliferative potential[116]. Of note, *Peg3* also promotes nuclear factor kappa-B (NFκB) activation[117], a pathway we previously identified as an essential regulator of angiogenesis during alveolarization[111, 118]. Transition of *Car4*- MEC from the early to late phenotype was marked by a down-regulation of angiogenic genes and up-regulation of genes that promote vascular stability, as well as an overall downregulation of gene expression, consistent with the transition from activation to quiescence as alveolarization and angiogenesis slows. Taken together, these data support a key role for the *Car4*- MEC in the expansion of the pulmonary circulation occurring during alveolarization.

We also identified developmental alterations in the transcriptome of the *Car4*+ MEC, specialized EC associated with type 1 alveolar epithelial cells[67]. *Car4*+ MEC highly express VEGFR2, and require epithelial-derived VEGF for survival. *Hoxa5* was suppressed in *Car4*+ MEC, providing a potential mechanism for their heightened VEGFR2 expression. During late sacculation, *Car4*+ MEC highly expressed genes related to ameboid cell migration and cytoskeletal rearrangement, perhaps reflecting dynamic extension of the multiple projections

extending from these EC to encircle the alveolus[115]. By P7, genes related to cytoskeletal rearrangement decreased, and genes related to vascular development increased, suggesting an important, but previously unrecognized role for *Car4*+ MEC in regulating vascular growth during early alveolarization. By late alveolarization, vascular development genes were down-regulated, and genes important for antigen presentation and response to interferon increased, indicating that *Car4*+ MEC subsume a greater role in immunity as the lung matures. This notion is further supported by the decrease in the expression of *Prdm1* from P1 to P21, a TF that promotes immune tolerance in other cells types. Taken together, these data reveal dynamic progression of *Car4*+ MEC phenotype with maturation, and identify putative functions for this subtype unique to the immature lung.

Proliferative EC, although completely absent in the mature lung, were relatively common in the immature lung, with two waves of lung EC proliferation: one just prior to birth, and a second at the onset of alveolarization. The proliferating EC lack *Car4* and other distinguishing genes expressed by *Car4*+ MECs, and many expressed *Peg3*, suggesting that proliferating EC are a subset of *Car4*- MEC, potentially responsible for replenishment of the *Car4*- MEC niche. The absence of proliferating *Car4*+ MEC is consistent with the hypothesis that *Car4*+ MEC differentiate from non-proliferative *Car4*- MECs [115]. Several TF families were enriched in the proliferative cluster, and *Mybl2* was required for proliferation of early alveolar primary MEC, suggesting a novel lineage-specific regulatory landscape. However, the mechanisms driving these separate waves of proliferation remain to be fully defined. Further elucidation of the mechanisms driving EC proliferation via ATAC Seq and ChIP Seq would be an important next step, given that augmentation of proliferation represents a promising therapy for diseases marked by impaired angiogenesis (e.g. BPD) or EC loss (e.g. ARDS).

Ongoing lung parenchymal and vascular growth after birth increases the susceptibility to injuries that disrupt development. This is most commonly observed in premature infants who develop BPD, a chronic lung disease characterized by impaired alveolarization and angiogenesis. The lungs of neonatal mice are structurally immature at birth, and exposure to hyperoxia recapitulates many of the features of BPD. In our study, hyperoxia induced multiple alterations in the endothelial transcriptome. First, a new cluster of proliferating venous EC appeared, suggesting that hyperoxia may induce aberrant proliferation of the venous endothelium. This finding is intriguing, as a certain subpopulation of infants with BPD develop pulmonary vein stenosis, a complication with associated high mortality, and pathobiologic mechanisms that remain poorly defined[119]. Second, hyperoxia induced a common gene signature across all EC subtypes characterized broadly by an up-regulation of genes that suppress cell growth and proliferation, and down-regulation of genes that promote angiogenesis and EC fate, providing novel potential mechanisms for the impaired angiogenesis observed in the hyperoxia-exposed lung. Third, hyperoxia induced distinct alterations in select MEC subtypes, including a suppression of MHC class I expression in both *Car4*- and proliferating MEC, suggesting a suppression of adaptive immune responses or induction of local tolerance in the hyperoxic lung[120]. This finding may have important clinical implications, as lung infections represent a source of secondary injury in patients with BPD, further increasing respiratory morbidity. Fourth, hyperoxia induced persistence of embryonic EC and decreased the abundance of late *Car4*- MEC, consistent with the arrest in lung development apparent histologically.

Hyperoxia also disrupted potential cross-talk between EC subtypes and between EC and immune cells. A clear hierarchy of cell types was seen with EC-EC interactions, particularly during early alveolarization, and this hierarchy was flattened by hyperoxia, indicating a loss of

specificity in terms of paracrine signaling. Hyperoxia also dysregulated *Car4*+ and *Car4*- MEC cross-talk, including *Apln*/*Aplnr* and *Kit*/*Kitl* signaling, causing both suppression and aberrant expression of key targets. Putative interactions between EC and immune cells also changed across development, and were altered by hyperoxia. Interactions between basophils and multiple EC subtypes were high prior to birth, with basophils and mast cells secreting ligands for canonical pathways regulating vascular development. Basophils play an essential role in directing alveolar macrophage differentiation during early postnatal lung development[13], and our data suggest that the basophils may also play an important, but previously unreported role in regulating pulmonary vascular growth. Hyperoxia increased the number of putative interactions between the EC and immune cells, particular in the macrophages subtype, Mac IV, suggesting a key role for this macrophage subtype in driving the hyperoxic immune response in the immature lung.

Our study has a number of limitations. First, marked changes occurred in the transcriptome between our final two timepoints, P7 and P21, precluding our ability to identify the discrete transcriptomic and phenotypic alterations occurring within this developmental window. Second, our data only included a single hyperoxic timepoint, limiting our capacity to elucidate early alterations that may underlie the phenotypic observed by P7. Further, we did not include timepoints after recovery from hyperoxia that would permit an assessment of the durability of these transcriptomic alterations, and identification of potential mechanisms driving the pathologic pulmonary vascular remodeling that occurs weeks after recovery from hyperoxia. Finally, the inclusion of a single male and female mouse per timepoint limited our ability to identify potential sex-dependent transcriptomic differences during development and injury. This represents an important area for future research given the well-known sexual dimorphism observed in both the

incidence and severity of BPD, as well is in the vascular response to hyperoxic injury observed in preclinical studies[121].

In summary, this study is the first to provide an in-depth atlas of the diversity of pulmonary EC during a period of rapid postnatal lung growth. Our data highlight the unique phenotype of immature pulmonary EC at both the macro and microvascular level, and comprehensively identify potential pathways and EC subtypes driving postnatal growth of the pulmonary circulation and the progression towards quiescence. Further, our data provides a substantially more granular report of the response of the pulmonary endothelium to hyperoxic injury than previously published, including the identification of select EC subtypes with a heightened susceptibility to injury. Taken together, our data provides an essential framework for understanding how the immature lung differs from the mature lung at single cell resolution, with important implications for diseases characterized by impaired lung and vascular growth, pathologic vascular remodeling, and lung injury.

Acknowledgements

We thank Sai Saroja Kolluru (Stanford University) for assistance with library submission to the Chan Zuckerberg Biohub, and Astrid Gillich for technical support with the RNAscope experiments. This work was supported by National Institutes of Health grants HL122918 (CMA), HD092316 (CMA, DNC), the Stanford Maternal Child Health Institute Tashia and John Morgridge Faculty Scholar Award (CMA), the Stanford Center of Excellence in Pulmonary Biology (DNC), Bill and Melinda Gates Foundation (SRQ), and the Chan Zuckerberg Biohub (DNC and SRQ). MAS is supported by the NSF-GRFP.

Sources of Funding

This work was supported by National Institutes of Health grants HL122918 (CMA), HD092316 (CMA, DNC), the Stanford Maternal Child Health Institute Tashia and John Morgridge Faculty Scholar Award (CMA), the Stanford Center of Excellence in Pulmonary Biology (DNC), Bill and Melinda Gates Foundation (SRQ), and the Chan Zuckerberg Biohub (DNC and SRQ).

Disclosures: None.

Figure Legends:

Fig. 1. Pulmonary endothelial heterogeneity increases after birth (A) Overview of the experimental design including the four timepoints (E18.5, P1, P7, P21) corresponding to key stages in late lung development. In separate studies, pups were maintained in chronic hyperoxia until P7. Lungs were isolated, perfused, and digested and endothelial cells isolated by fluorescence activated cell sorting (FACS) for the dead-stain-, CD326-CD45-CD31+ population. (B) UMAP and unsupervised clustering of 2931 endothelial cells identified 9 transcriptionally distinct EC subpopulations present during the lung from the early saccular to late alveolar stages of development. (C) Dot plot showing level of expression (purple to yellow), and fraction of the population expressing the particular gene (dot size) for distinguishing genes expressed by the Leiden clusters. (D) UMAP of EC clusters identifying developmental timepoint of cell origin with E18.5 (blue), P1 (yellow), P7 (orange) and P21 (red). (E) UMAP plots of genes expressed predominantly before (E) and (F) after birth. For (E) and (F), the color scale is a logarithmic scale with a pseudocount of 0.1 counts per million, normalized to the highest expressing cell.

Figure 2. Pulmonary EC in the perinatal lung are transcriptionally distinct from the adult. This data set and lung data from Tabula Muris (TM), which focused on three-month old mice, were merged, restricted to genes that were overlapping, normalized to counts per million reads, feature selected and subjected to PCA, followed by UMAP. UMAP plots of (A) data source (B) cell type and (C) developmental stage using our data combined with Tabula Muris,.

Figure 3. Two transcriptionally distinct arterial subtypes are present in the perinatal lung UMAP plots of genes highly expressed by (A) lymphatic EC, (B) venous EC, and (C) arterial EC I and II, with gene expression colored logarithmically as described above. (D) Quantification of the abundance of each macrovascular EC subset at each developmental timepoint expressed on a logarithmic scale as percentage of total macrovascular EC. (E) Multiplexed *in situ* hybridization to detect gene expression of *Cdh5* (green), *Gja5* (white) and *Dkk2* (red) in lung tissue from mice at P1. Cal bar=20µm. (F) Pathway analysis performed via Metscape on the top 100 up-regulated genes in the arterial I and (G) arterial II clusters, respectively. (H) Heatmap of select differentially expressed genes in arterial I and II within enriched pathways illustrated. The color scale is logarithmic counts per million, normalized to the highest expressing population for each gene. (I) Cumulative distributions of gene expression in arterial II EC, colored by timepoint.

Figure 4. ***Pulmonary microvascular EC diversity increases during early postnatal life***

(A) UMAP plots of genes highly expressed in non-proliferative embryonic MEC, with gene expression colored logarithmically as described above. (B) Relative abundance of embryonic, early *Car4*-, and late *Car4*- MEC at each developmental timepoint expressed on a logarithmic scale as percentage of total EC. (C) RNA velocity demonstrating a transition from early to late

Car4- EC. (D) UMAP for *Peg3* (left) and multiplex *in situ* hybridization (middle) to detect *Peg3* (red) and *Cdh5* (green) in lung tissue at P7 and P21. Calibration bar=20μm. Quantification (right) of the percent of *Peg3*+ EC versus total EC in lung sections from P7 and P21 mice (31.4±1.6 vs. 10.3±0.55 and P=0.002 by t-test with n=3 per group). (E) Cumulative distribution of number of expressed genes, indicating early *Car4*- MEC express more genes than late *Car4*- capillaries. (F) Heatmap of genes differentially expressed between early and late *Car4*- capillaries, grouped by pathway.

Figure 5. Car4+ MEC exhibit dynamic changes in gene expression to influence cell migration, angiogenesis and immunity. (A) UMAP plots of genes highly expressed *Car4*+ MEC. (B) Multiplex *in situ* hybridization to detect gene expression of *Car4* (white), *Tbx2* (red), and *Cdh5* (green) with DAPI (blue). Calibration bar=20μm. (C) UMAP plot*s of genes encoding TFs positively (top) and negatively (bottom) correlated with Tbx2 in the* Car4+ MEC. (D) UMAP embedding of *Car4*+ MEC colored by timepoint (left), by pseudotime starting from the bottom-right corner with an average trajectory (middle), and will all EC in green with RNA overlayed (right). All three methods indicate maturation along the developmental axis. (E) Single cell (dots) and average (lines) expression of genes increasing and decreasing across peudotime in the *Car4*+ MEC. The y axis uses $\log_{10}$ scale of expression normalized to the highest expressing cell. (F-I) Pathway analysis of DEG in the *Car4*+ MEC between each of the postnatal timepoints. (J) Heatmap of select DEG in *Car4*+ MEC across pseudotime within enriched pathways. UMAP plots with gene expression colored logarithmically as described above.

Figure 6. Proliferating EC peak just prior to birth and again during early alveolarization.

(A) UMAP plots of select genes highly expressed by proliferating EC. (B) Relative abundance of proliferating EC at each developmental timepoint expressed on a logarithmic scale as percentage of total EC. (C) Multiplex *in situ* hybridization to detect *Mki67*(red) and *Cdh5* (green) in lung tissue at P7. Calibration bar=20μm. (D) Sankey diagrams of transcription factors (TF) families enriched in TFs upregulated in non-proliferative ECs compared to all TFs (left) and in TFs upregulated in proliferative ECs versus all TFs. (E) Cumulative distribution of 100 simulations computing enrichment of TF families when picking random TFs (black line), compared with the actual enrichment TFs upregulated in proliferative ECs (red line). (F) Table of enrichment factors for each TF family in proliferating EC versus all TFs as shown in (D) and nonparametric P-value as in (E), limited to the most enriched or depleted TF families.(G) UMAP plot of *Mybl2* expression indicating expression in P7 proliferative EC cells (top right). (H) BrdU incorporation assay to determine proliferation in primary pulmonary EC obtained from the P7 lung, transfected with NTC or *Mybl2* siRNA maintained in starvation or EC growth media for 24h. Data presented are mean±SEM with n=6 and *P<0.05 and ****P<0.0001 vs. starvation, and ####P<0.0001 vs. NTC. (I) Representative images of primary PEC transfected with NTC and *Mybl2* siRNA subjected to IHC to detect active caspase-3 (red), CD31 (green) and Dapi (blue). Calibration bar=50μm. UMAP plots with gene expression colored logarithmically as described above.

Figure 7: Chronic hyperoxia disrupts the transcriptome of specific endothelial subsets and delays microvascular maturation. (A) UMAP and unsupervised clustering of EC derived from the P7 lung maintained in normoxia and hyperoxia identified 9 transcriptionally distinct clusters. (B) UMAP plot colored by treatment condition. (C) Relative abundance of EC as a fraction of total EC in normoxia versus hyperoxia. The y axis has a logarithmic scale. (D-E) Identification of

common up- (D) and down- (E) regulated genes in hyperoxia. In each plot, the start of the arrow corresponds to the average expression of the gene in normoxia, and the tip of the arrow corresponds to the average expression of the gene in that cluster in hyperoxia. The y axis uses a logarithmic scale of gene expression in cpm. (F) Heat map of select up- and down- regulated genes in hyperoxia versus normoxia at P7 in the early *Car4*- MEC (top), the *Car4*+ MEC (middle), and proliferative EC (bottom). Values in each square represent the log2 fold changes in average expression. (G) Representative multiplex in situ hybridization to detect *Cdh5* (green) and *Ntrk2* (red) in combination with Dapi (blue). Calibration bar=20μm. (H) Representative multiplex in situ hybridization to detect *Cdh5* (green) *Inhba* (red), and *Car4* (white) in combination with Dapi (blue). Calibration bar=20μm.

Figure 8: Alterations in cell communication within endothelial subtypes and between EC and immune cells during development and in response to injury. (A) Number of interactions detected for each EC subtype at each time point (left) and in normoxia versus hyperoxia at P7 (right). (B) Heatmap of the number interactions detected between each pair of cell types within the endothelium for each time point. (C) Triangle plot (left) indicating simultaneously the number of interactions detected between each pair of cell types at P7 in normoxia (color) and the change in number caused by hyperoxia (triangle size and direction). Heatmap (right) of the resulting number of interactions, showing that hyperoxia interactions lose much of their cell type-specific structure. (D) Average expression of *Apln*/*Kitl* (top/bottom, respectively) in *Car4*+ MEC and *Aplnr*/*Kit* in *Car4*- MEC at each time point (left) and at P7 in normoxia versus hyperoxia (right). (E) Heatmap of the number of interactions detected between endothelial and immune cell types at each time point. (F) Distributions of *Cxcl12* expression in arterial EC (I + II) and *Car4*- MEC at each time

point (top) and average expression of its receptors *Cxcr4* and *Ackr3* in the main expressing cell types (bottom). (G) Heatmap of endothelial-immune detected interactions in hyperoxia, colored as in (E).

Methods:

Mouse lung cell isolation. C57BL/6 mice were obtained from Charles River Laboratories. For studies using E18.5, P1, and P7 murine lungs, pregnant dams were purchased, and pups aged prior to lung isolation. At E18.5, dam was asphyxiated with CO2 and pups extracted. At P1, P7, and P21 pups were euthanized with euthanasia solution (Vedco Inc.). Genetic sex of mice at developmental stages E18.5 and P1 was determined by performing PCR amplification of the Y chromosome gene Sry. P7 and P21 mice were sexed through identification of a pigment spot on the scrotum of male mice[122]. For all timepoints, female and male mice were randomly selected for the studies. For all timepoints, except E18.5, the pulmonary circulation was perfused with ice cold heparin in 1x PBS until the circulation was cleared of blood. Lungs were minced and digested with Liberase (Sigma Aldrich) in RPMI for 15 (E18.5, P1, and P7) or 30 (P21) minutes at 37C, 200 rpm. Lungs were manually triturated and 5% fetal bovine serum (FBS) in 1x PBS was used to quench liberase solution. Red blood cells were lysed with 1x RBC lysis buffer (Invitrogen) as indicated by the manufacturer and total lung cells counted on Biorad cell counter (BioRad). Protocols for the murine studies adhered to American Physiological Society/US National Institutes

of Health guidelines for humane use of animals for research and were prospectively approved by the Institutional Animal Care and Use Committee at Stanford (APLAC #19087).

Chronic Hyperoxia. Newborn C57BL/6 mice pups at P0 were maintained in 80% O_2 (hyperoxia) in a BioSpherix chamber (BioSpherix, Parish, NY) for 7 days, an established experimental model that recapitulates the impaired alveolarization observed in BPD[123]. Dams were rotated every 24h to prevent oxygen toxicity. Pups were euthanized at P7 and single lung cells obtained as described above.

Immunostaining and fluorescence-activated cell sorting (FACS) of single cells. Lungs were plated at $1x10^6$ cells per well and stained with Fc block (CD16/32, 1:100, Tonbo Biosciences) for 30 min on ice. Cells were surface stained with the endothelial marker CD31 (1:100, clone: MEC3.1, eBiosciences), epithelial marker CD326 (1:100, clone: CD326, eBiosciences), and immune marker CD45 (1:100, clone: F11, eBiosciences) for 30 min on ice. The live/dead dye, Sytox Blue (Invitrogen), was added to cells and incubated for 3 min prior to sorting into 384-well plates (Bio-Rad Laboratories, Inc) prefilled with lysis buffer using the Sony LE-SH800 cell sorter (Sony Biotechnology Inc), a 100µm sorting chip (Catalog number: LE-C3110) and ultra-purity mode. Single color controls were used to perform fluorescence compensation and generate sorting gates. 384-well plates containing single cells were spun down, immediately placed on dry ice and stored at -80C.

cDNA library generation using Smart-Seq2. Complementary DNA from sorted cells was reverse transcribed and amplified using the Smart-Seq2 protocol on 384-well plates as previously

described[124, 125]. Concentration of cDNA was quantified using picogreen (Life technology corp.) to ensure adequate cDNA amplification. In preparation for library generation, cDNA was normalized to 0.4 ng/uL. Tagmentation and barcoding of cDNA was prepared using in-house Tn5 transposase and custom, double barcoded indices[10]. Library fragment concentration and purity were quantified by Agilent bioanalyzer. Libraries were pooled and sequenced on Illumina NovaSeq 6000 with 2x100 base kits and at a depth of around 1 million read pairs per cell.

Data analysis and availability. Sequencing reads were mapped against the mouse genome (GRCm38) using STAR aligner[126] and gene were counted using HTSeq[127]. FZ has been the main maintainer of HTSeq for several years. To coordinate mapping and counting on Stanford's high-performance computing cluster, snakemake was used[128]. Gene expression count tables were converted into loom objects (https://linnarssonlab.org/loompy/) and cells with less than 50,000 uniquely mapped reads or less than 400 genes per cell were discarded. Doublets were removed in three ways. First, clusters that expressed epithelial, endothelial or mesenchymal genes were excluded. Clusters showing joint expression of mutually exclusive cell type markers (e.g. *Epcam*, *Ptprc*, *Col6a2*) with *Cdh5* were manually excluded as well. Finally, a few remaining doublets were removed manually. Counts for the remaining 2931 cells were normalized to counts per million reads. For Uniform Manifold Approximation and Projection (UMAP)[16], 500 features were selected that had a high Fano factor in most mice, and the restricted count matrix was log-transformed with a pseudocount of 0.1 and projected onto the top 25 principal components using scikit-learn[129]. Unsupervised clustering was performed using Leiden[130]. Singlet (https://github.com/iosonofabio/singlet) and for specific analyses, custom Python 3 scripts were used: the latter available at https://github.com/iosonofabio/lung_neonatal_endothelial. Pathway

analysis was performed using Metascape[131]. Pseudotime was determined with Scanpy: https://scanpy.readthedocs.io/en/stable/api/scanpy.tl.dpt.html?highlight=pseudotime#scanpy.tl.dpt. RNA velocity was performed[54] using scVelo, which explicitly models curly developmental trajectories (https://www.biorxiv.org/content/10.1101/820936v1). Data from Tabula Muris[78] was downloaded from Figshare. Raw fastq files, count tables, and metadata are available on NCBI's Gene Expression Omnibus (GEO) under submission GSE159804. https://www.ncbi.nlm.nih.gov/geo/query/acc.cgi?acc=GSE159804

In-situ validation using RNAscope and immunofluorescence (IF). Embryonic and post-natal mice were euthanized as described above. Female and male mice were randomly selected from the litter, and at least 2 litters were used to source the lung tissue for all validation studies. P1, P7, and P21 murine lungs were perfused as described above, and P7 and P21 lungs inflated with 2% low melting agarose (LMT) in 1xPBS and placed in 10% neutral buffered formalin. Following 20 hours incubation at 4C, fixed lungs were washed twice in 1xPBS and placed in 70% ethanol for paraffin-embedding. In situ validation of genes identified by scRNAseq was performed using the RNAscope Multiplex Fluorescent v2 Assay kit (Advanced Cell Diagnostics) and according to the manufacturer's protocol. Formalin-fixed paraffin-embedded (FFPE) lung sections (5 μm) were used within a day of sectioning for optimal results. Nuclei were counterstained with DAPI (Life Technology Corp.) and extracellular matrix proteins stained with hydrazide[132]. Opal dyes (Akoya Biosciences) were used for signal amplification as directed by the manufacturer. Images were captured with Zeiss LSM 780 and Zeiss LSM 880 confocal microscopes, using 405nm, 488nm, 560nm and 633nm excitation lasers. For scanning tissue, each image frame was set as 1024x1024

and pinhole 1AiryUnit (AU). For providing Z-stack confocal images, the Z-stack panel was used to set z-boundary and optimal intervals, and images with maximum intensity were processed by merging Z-stacks images. For all both merged signal and split channels were collected.

Quantification of RNA Scope Images. For select RNA scope experiments, the number and location of specific cells were quantified. Adjustments to the brightness and contrast of an image to increase the clarity of the signal was always applied to the entire image and never to separate areas of the image. For the determination of the percentage of *Peg3*$^{+}$ cells located in the distal lung parenchyma, at least 4 separate images were quantified per mouse. For all quantification analysis, a cell was deemed positive if it contained >1 puncta per cell for a specific gene.

Isolation of Primary Lung Microvascular EC. PEC were isolated from P7 C57BL/6 mice as we have described previously[111]. Briefly, primary MEC were obtained from 10-12 mouse lungs by digestion of peripheral lung tissue with collagenase IA (0.5 mg/ml, Sigma, St. Louis, MO) for 30 min at 37°C, followed by incubating cell lysate for 15 min at RT with anti-CD31-coated magnetic beads (Dynabeads, Invitrogen, Carlsbad, CA), resulting in between 2-3 million MEC after bead selection. MEC isolated by this method were previously characterized by flow cytometry and found to be exclusively CD45- , greater than 95% positive for the endothelial specific marker, CD102 (E2), and greater than 80% demonstrating binding to Griffonia simplicifolia, indicating primarily microvascular EC. Primary MEC were cultured in endothelial growth media (EGM) containing 5% FBS with growth factors (EBM-2; Lonza, Basel, Switzerland) at 37°C in 5% CO_2. PEC from passage 0-2 were used for all experiments.

RNA Interference: Primary lung MEC isolated from P7 mice were transfected with 25 nM of NTC, or Mybl2 On-Target Plus SMART pool siRNA (Dharmacon, Lafayette, CO; Thermo Fisher Scientific, Lafayette, CO) using Lipofectamine 2000 (Invitrogen) for 6h as previously described (E8). The groups of MEC were then recovered for 42h, prior to use for proliferation assays and immunocytochemistry.

Proliferation Assays. Proliferation of siRNA transfected primary lung MEC proliferation was determined by BrdU incorporation assays. MEC (6×10^3) were plated into each well of a 96-well plate and synchronized with starvation media (0.2% FBS) for 16h, prior to stimulation with experimental media. The incorporation of BrdU was then measured by ELISA at 24h per the manufacturer's protocol (Roche Diagnostics, Mannheim, Germany).

Active caspase-3 Immunocytochemistry. siRNA transfected primary lung MEC were gown on $22mm^2$ coverslips placed in a 6-well cell culture plate. Cells were fixed with 3.2% paraformaldehyde and air-dried. Cells were rehydrated and immunocytochemistry performed as previously described using primary antibodies against active caspase-3 (Abcam, Cambridge, MA) overnight at 4°C, prior to incubation with secondary antibody and Hoechst reagent. Fluorescent images were captured and quantified using either the Keyence BZ-X700/BZ-X710 Microscope, and Metamorph Image analysis software (Molecular Devices, Sunnyvale, CA).

Statistical Analyses. To identify differentially expressed genes within cell populations, Kolmogorov Smirnov tests on the distributions of gene expression were performed on all genes, and the genes with the largest test statistic (lowest P value) were chosen as the top differentially

expressed genes. For the flow cytometry studies of lung lymphocytes, 7-8 mice were in each group. Data are presented as mean ± SD. Differences between groups was determined by Student's t-test with a P value of ≤0.05 considered statistically significant.

References:

[1] Lakshminrusimha S, Steinhorn RH. Pulmonary vascular biology during neonatal transition. Clin Perinatol. 1999;26:601-19.
[2] Burri PH, Tarek MR. A novel mechanism of capillary growth in the rat pulmonary microcirculation. Anat Rec. 1990;228:35-45.
[3] Zeltner TB, Burri PH. The postnatal development and growth of the human lung. II. Morphology. Respir Physiol. 1987;67:269-82.
[4] Zeltner TB, Caduff JH, Gehr P, Pfenninger J, Burri PH. The postnatal development and growth of the human lung. I. Morphometry. Respir Physiol. 1987;67:247-67.
[5] Jobe AH. The new bronchopulmonary dysplasia. Curr Opin Pediatr. 2011;23:167-72.
[6] Toya SP, Malik AB. Role of endothelial injury in disease mechanisms and contribution of progenitor cells in mediating endothelial repair. Immunobiology. 2012;217:569-80.
[7] Kawasaki T, Nishiwaki T, Sekine A, Nishimura R, Suda R, Urushibara T, et al. Vascular Repair by Tissue-Resident Endothelial Progenitor Cells in Endotoxin-Induced Lung Injury. Am J Respir Cell Mol Biol. 2015;53:500-12.
[8] Thane K, Ingenito EP, Hoffman AM. Lung regeneration and translational implications of the postpneumonectomy model. Transl Res. 2013.
[9] Jancelewicz T, Grethel EJ, Chapin CJ, Clifton MS, Nobuhara KK. Vascular endothelial growth factor isoform and receptor expression during compensatory lung growth. J Surg Res. 2010;160:107-13.
[10] Tabula Muris C, Overall c, Logistical c, Organ c, processing, Library p, et al. Single-cell transcriptomics of 20 mouse organs creates a Tabula Muris. Nature. 2018;562:367-72.
[11] Travaglini KJ, Nabhan AN, Penland L, Sinha R, Gillich A, Sit RV, et al. A molecular cell atlas of the human lung from single-cell RNA sequencing. Nature. 2020;587:619-25.
[12] Treutlein B, Brownfield DG, Wu AR, Neff NF, Mantalas GL, Espinoza FH, et al. Reconstructing lineage hierarchies of the distal lung epithelium using single-cell RNA-seq. Nature. 2014;509:371-5.
[13] Cohen M, Giladi A, Gorki AD, Solodkin DG, Zada M, Hladik A, et al. Lung Single-Cell Signaling Interaction Map Reveals Basophil Role in Macrophage Imprinting. Cell. 2018;175:1031-44 e18.
[14] Domingo-Gonzalez R, Zanini F, Che X, Liu M, Jones RC, Swift MA, et al. Diverse homeostatic and immunomodulatory roles of immune cells in the developing mouse lung at single cell resolution. Elife. 2020;9.
[15] Su T, Stanley G, Sinha R, D'Amato G, Das S, Rhee S, et al. Single-cell analysis of early progenitor cells that build coronary arteries. Nature. 2018;559:356-62.
[16] Becht E, McInnes L, Healy J, Dutertre CA, Kwok IWH, Ng LG, et al. Dimensionality reduction for visualizing single-cell data using UMAP. Nat Biotechnol. 2018.
[17] Traag VA, Waltman L, van Eck NJ. From Louvain to Leiden: guaranteeing well-connected communities. Sci Rep-Uk. 2019;9.
[18] Jurisic G, Iolyeva M, Proulx ST, Halin C, Detmar M. Thymus cell antigen 1 (Thy1, CD90) is expressed by lymphatic vessels and mediates cell adhesion to lymphatic endothelium. Exp Cell Res. 2010;316:2982-92.
[19] Wigle JT, Harvey N, Detmar M, Lagutina I, Grosveld G, Gunn MD, et al. An essential role for Prox1 in the induction of the lymphatic endothelial cell phenotype. EMBO J. 2002;21:1505-13.

[20] Hromas R, Kim CH, Klemsz M, Krathwohl M, Fife K, Cooper S, et al. Isolation and characterization of Exodus-2, a novel C-C chemokine with a unique 37-amino acid carboxyl-terminal extension. J Immunol. 1997;159:2554-8.
[21] Aranguren XL, Beerens M, Vandevelde W, Dewerchin M, Carmeliet P, Luttun A. Transcription factor COUP-TFII is indispensable for venous and lymphatic development in zebrafish and Xenopus laevis. Biochem Biophys Res Commun. 2011;410:121-6.
[22] You LR, Lin FJ, Lee CT, DeMayo FJ, Tsai MJ, Tsai SY. Suppression of Notch signalling by the COUP-TFII transcription factor regulates vein identity. Nature. 2005;435:98-104.
[23] Buschmann I, Pries A, Styp-Rekowska B, Hillmeister P, Loufrani L, Henrion D, et al. Pulsatile shear and Gja5 modulate arterial identity and remodeling events during flow-driven arteriogenesis. Development. 2010;137:2187-96.
[24] Ekman N, Lymboussaki A, Vastrik I, Sarvas K, Kaipainen A, Alitalo K. Bmx tyrosine kinase is specifically expressed in the endocardium and the endothelium of large arteries. Circulation. 1997;96:1729-32.
[25] Deckelbaum RA, Lobov IB, Cheung E, Halasz G, Rajamani S, Lerner J, et al. The potassium channel Kcne3 is a VEGFA-inducible gene selectively expressed by vascular endothelial tip cells. Angiogenesis. 2020;23:179-92.
[26] Gage PJ, Qian M, Wu D, Rosenberg KI. The canonical Wnt signaling antagonist DKK2 is an essential effector of PITX2 function during normal eye development. Dev Biol. 2008;317:310-24.
[27] Kuhn K. Basement membrane (type IV) collagen. Matrix Biol. 1995;14:439-45.
[28] Wernert N, Raes MB, Lassalle P, Dehouck MP, Gosselin B, Vandenbunder B, et al. c-ets1 proto-oncogene is a transcription factor expressed in endothelial cells during tumor vascularization and other forms of angiogenesis in humans. Am J Pathol. 1992;140:119-27.
[29] Wei G, Srinivasan R, Cantemir-Stone CZ, Sharma SM, Santhanam R, Weinstein M, et al. Ets1 and Ets2 are required for endothelial cell survival during embryonic angiogenesis. Blood. 2009;114:1123-30.
[30] Bedell VM, Yeo SY, Park KW, Chung J, Seth P, Shivalingappa V, et al. roundabout4 is essential for angiogenesis in vivo. Proc Natl Acad Sci U S A. 2005;102:6373-8.
[31] Ren X, Ustiyan V, Guo M, Wang G, Bolte C, Zhang Y, et al. Postnatal Alveologenesis Depends on FOXF1 Signaling in c-KIT(+) Endothelial Progenitor Cells. Am J Respir Crit Care Med. 2019.
[32] Matsui J, Wakabayashi T, Asada M, Yoshimatsu K, Okada M. Stem cell factor/c-kit signaling promotes the survival, migration, and capillary tube formation of human umbilical vein endothelial cells. J Biol Chem. 2004;279:18600-7.
[33] Roberts DM, Anderson AL, Hidaka M, Swetenburg RL, Patterson C, Stanford WL, et al. A vascular gene trap screen defines RasGRP3 as an angiogenesis-regulated gene required for the endothelial response to phorbol esters. Mol Cell Biol. 2004;24:10515-28.
[34] van Breevoort D, van Agtmaal EL, Dragt BS, Gebbinck JK, Dienava-Verdoold I, Kragt A, et al. Proteomic screen identifies IGFBP7 as a novel component of endothelial cell-specific Weibel-Palade bodies. J Proteome Res. 2012;11:2925-36.
[35] Hooper AT, Shmelkov SV, Gupta S, Milde T, Bambino K, Gillen K, et al. Angiomodulin is a specific marker of vasculature and regulates vascular endothelial growth factor-A-dependent neoangiogenesis. Circ Res. 2009;105:201-8.

[36] Hu L, Zang MD, Wang HX, Li JF, Su LP, Yan M, et al. Biglycan stimulates VEGF expression in endothelial cells by activating the TLR signaling pathway. Mol Oncol. 2016;10:1473-84.
[37] Kozel BA, Mecham RP. Elastic fiber ultrastructure and assembly. Matrix Biol. 2019;84:31-40.
[38] Pedrosa AR, Trindade A, Fernandes AC, Carvalho C, Gigante J, Tavares AT, et al. Endothelial Jagged1 antagonizes Dll4 regulation of endothelial branching and promotes vascular maturation downstream of Dll4/Notch1. Arterioscler Thromb Vasc Biol. 2015;35:1134-46.
[39] Yuan L, Le Bras A, Sacharidou A, Itagaki K, Zhan Y, Kondo M, et al. ETS-related gene (ERG) controls endothelial cell permeability via transcriptional regulation of the claudin 5 (CLDN5) gene. J Biol Chem. 2012;287:6582-91.
[40] Dabovic B, Robertson IB, Zilberberg L, Vassallo M, Davis EC, Rifkin DB. Function of latent TGFbeta binding protein 4 and fibulin 5 in elastogenesis and lung development. J Cell Physiol. 2015;230:226-36.
[41] Michalczyk ER, Chen L, Fine D, Zhao Y, Mascarinas E, Grippo PJ, et al. Pigment Epithelium-Derived Factor (PEDF) as a Regulator of Wound Angiogenesis. Sci Rep. 2018;8:11142.
[42] Park H, Jung HY, Choi HJ, Kim DY, Yoo JY, Yun CO, et al. Distinct roles of DKK1 and DKK2 in tumor angiogenesis. Angiogenesis. 2014;17:221-34.
[43] Gocheva V, Chen X, Peters C, Reinheckel T, Joyce JA. Deletion of cathepsin H perturbs angiogenic switching, vascularization and growth of tumors in a mouse model of pancreatic islet cell cancer. Biol Chem. 2010;391:937-45.
[44] Salcher S, Hermann M, Kiechl-Kohlendorfer U, Ausserlechner MJ, Obexer P. C10ORF10/DEPP-mediated ROS accumulation is a critical modulator of FOXO3-induced autophagy. Mol Cancer. 2017;16:95.
[45] Chen S, Gai J, Wang Y, Li H. FoxO regulates expression of decidual protein induced by progesterone (DEPP) in human endothelial cells. FEBS Lett. 2011;585:1796-800.
[46] Naschberger E, Liebl A, Schellerer VS, Schutz M, Britzen-Laurent N, Kolbel P, et al. Matricellular protein SPARCL1 regulates tumor microenvironment-dependent endothelial cell heterogeneity in colorectal carcinoma. J Clin Invest. 2016;126:4187-204.
[47] Cui XB, Guo X, Chen SY. Response gene to complement 32 deficiency causes impaired placental angiogenesis in mice. Cardiovasc Res. 2013;99:632-9.
[48] Mayer W, Hemberger M, Frank HG, Grummer R, Winterhager E, Kaufmann P, et al. Expression of the imprinted genes MEST/Mest in human and murine placenta suggests a role in angiogenesis. Dev Dyn. 2000;217:1-10.
[49] Jung H, Lee SK, Jho EH. Mest/Peg1 inhibits Wnt signalling through regulation of LRP6 glycosylation. Biochem J. 2011;436:263-9.
[50] Zhou X, Xiao D. Long non-coding RNA GAS5 is critical for maintaining stemness and induces chemoresistance in cancer stem-like cells derived from HCT116. Oncol Lett. 2020;19:3431-8.
[51] Wang YN, Shan K, Yao MD, Yao J, Wang JJ, Li X, et al. Long Noncoding RNA-GAS5: A Novel Regulator of Hypertension-Induced Vascular Remodeling. Hypertension. 2016;68:736-48.
[52] Yao J, Shi Z, Ma X, Xu D, Ming G. lncRNA GAS5/miR-223/NAMPT axis modulates the cell proliferation and senescence of endothelial progenitor cells through PI3K/AKT signaling. J Cell Biochem. 2019;120:14518-30.

[53] Wang BB, Lu R, Wang WC, Jin Y. Inducible and reversible suppression of Npm1 gene expression using stably integrated small interfering RNA vector in mouse embryonic stem cells. Biochem Biophys Res Commun. 2006;347:1129-37.
[54] La Manno G, Soldatov R, Zeisel A, Braun E, Hochgerner H, Petukhov V, et al. RNA velocity of single cells. Nature. 2018;560:494-8.
[55] Relaix F, Weng X, Marazzi G, Yang E, Copeland N, Jenkins N, et al. Pw1, a novel zinc finger gene implicated in the myogenic and neuronal lineages. Dev Biol. 1996;177:383-96.
[56] Theka I, Sottile F, Aulicino F, Garcia AC, Cosma MP. Reduced expression of Paternally Expressed Gene-3 enhances somatic cell reprogramming through mitochondrial activity perturbation. Sci Rep. 2017;7:9705.
[57] Besson V, Smeriglio P, Wegener A, Relaix F, Nait Oumesmar B, Sassoon DA, et al. PW1 gene/paternally expressed gene 3 (PW1/Peg3) identifies multiple adult stem and progenitor cell populations. Proc Natl Acad Sci U S A. 2011;108:11470-5.
[58] Kim J, Shapiro MJ, Bamidele AO, Gurel P, Thapa P, Higgs HN, et al. Coactosin-like 1 antagonizes cofilin to promote lamellipodial protrusion at the immune synapse. PLoS One. 2014;9:e85090.
[59] Gaetano C, Catalano A, Illi B, Felici A, Minucci S, Palumbo R, et al. Retinoids induce fibroblast growth factor-2 production in endothelial cells via retinoic acid receptor alpha activation and stimulate angiogenesis in vitro and in vivo. Circ Res. 2001;88:E38-47.
[60] Babendreyer A, Molls L, Simons IM, Dreymueller D, Biller K, Jahr H, et al. The metalloproteinase ADAM15 is upregulated by shear stress and promotes survival of endothelial cells. J Mol Cell Cardiol. 2019;134:51-61.
[61] Xie B, Shen J, Dong A, Swaim M, Hackett SF, Wyder L, et al. An Adam15 amplification loop promotes vascular endothelial growth factor-induced ocular neovascularization. FASEB J. 2008;22:2775-83.
[62] Melter M, Reinders ME, Sho M, Pal S, Geehan C, Denton MD, et al. Ligation of CD40 induces the expression of vascular endothelial growth factor by endothelial cells and monocytes and promotes angiogenesis in vivo. Blood. 2000;96:3801-8.
[63] Dawson DW, Pearce SF, Zhong R, Silverstein RL, Frazier WA, Bouck NP. CD36 mediates the In vitro inhibitory effects of thrombospondin-1 on endothelial cells. J Cell Biol. 1997;138:707-17.
[64] Eble JA, Golbik R, Mann K, Kuhn K. The alpha 1 beta 1 integrin recognition site of the basement membrane collagen molecule [alpha 1(IV)]2 alpha 2(IV). EMBO J. 1993;12:4795-802.
[65] Jung B, Obinata H, Galvani S, Mendelson K, Ding BS, Skoura A, et al. Flow-regulated endothelial S1P receptor-1 signaling sustains vascular development. Dev Cell. 2012;23:600-10.
[66] Camerer E, Regard JB, Cornelissen I, Srinivasan Y, Duong DN, Palmer D, et al. Sphingosine-1-phosphate in the plasma compartment regulates basal and inflammation-induced vascular leak in mice. J Clin Invest. 2009;119:1871-9.
[67] Vila Ellis L, Cain MP, Hutchison V, Flodby P, Crandall ED, Borok Z, et al. Epithelial Vegfa Specifies a Distinct Endothelial Population in the Mouse Lung. Dev Cell. 2020;52:617-30 e6.
[68] Niethamer TK, Stabler CT, Leach JP, Zepp JA, Morley MP, Babu A, et al. Defining the role of pulmonary endothelial cell heterogeneity in the response to acute lung injury. Elife. 2020;9.
[69] Wakahara T, Kusu N, Yamauchi H, Kimura I, Konishi M, Miyake A, et al. Fibin, a novel secreted lateral plate mesoderm signal, is essential for pectoral fin bud initiation in zebrafish. Dev Biol. 2007;303:527-35.

[70] Mesbah K, Harrelson Z, Theveniau-Ruissy M, Papaioannou VE, Kelly RG. Tbx3 is required for outflow tract development. Circ Res. 2008;103:743-50.
[71] Barry DM, McMillan EA, Kunar B, Lis R, Zhang T, Lu T, et al. Molecular determinants of nephron vascular specialization in the kidney. Nat Commun. 2019;10:5705.
[72] Mould AW, Morgan MA, Nelson AC, Bikoff EK, Robertson EJ. Blimp1/Prdm1 Functions in Opposition to Irf1 to Maintain Neonatal Tolerance during Postnatal Intestinal Maturation. PLoS Genet. 2015;11:e1005375.
[73] Jain R, Li D, Gupta M, Manderfield LJ, Ifkovits JL, Wang Q, et al. HEART DEVELOPMENT. Integration of Bmp and Wnt signaling by Hopx specifies commitment of cardiomyoblasts. Science. 2015;348:aaa6071.
[74] Bahrami SB, Veiseh M, Dunn AA, Boudreau NJ. Temporal changes in Hox gene expression accompany endothelial cell differentiation of embryonic stem cells. Cell Adh Migr. 2011;5:133-41.
[75] Hosaka T, Biggs WH, 3rd, Tieu D, Boyer AD, Varki NM, Cavenee WK, et al. Disruption of forkhead transcription factor (FOXO) family members in mice reveals their functional diversification. Proc Natl Acad Sci U S A. 2004;101:2975-80.
[76] Kokubo H, Miyagawa-Tomita S, Nakazawa M, Saga Y, Johnson RL. Mouse hesr1 and hesr2 genes are redundantly required to mediate Notch signaling in the developing cardiovascular system. Dev Biol. 2005;278:301-9.
[77] Schulz B, Pruessmeyer J, Maretzky T, Ludwig A, Blobel CP, Saftig P, et al. ADAM10 regulates endothelial permeability and T-Cell transmigration by proteolysis of vascular endothelial cadherin. Circ Res. 2008;102:1192-201.
[78] Arthur HM, Ure J, Smith AJ, Renforth G, Wilson DI, Torsney E, et al. Endoglin, an ancillary TGFbeta receptor, is required for extraembryonic angiogenesis and plays a key role in heart development. Dev Biol. 2000;217:42-53.
[79] Junge HJ, Yang S, Burton JB, Paes K, Shu X, French DM, et al. TSPAN12 regulates retinal vascular development by promoting Norrin- but not Wnt-induced FZD4/beta-catenin signaling. Cell. 2009;139:299-311.
[80] Yang J, Joshi S, Wang Q, Li P, Wang H, Xiong Y, et al. 14-3-3zeta loss leads to neonatal lethality by microRNA-126 downregulation-mediated developmental defects in lung vasculature. Cell Biosci. 2017;7:58.
[81] Nikolic I, Stankovic ND, Bicker F, Meister J, Braun H, Awwad K, et al. EGFL7 ligates alphavbeta3 integrin to enhance vessel formation. Blood. 2013;121:3041-50.
[82] Jones PD, Kaiser MA, Ghaderi Najafabadi M, Koplev S, Zhao Y, Douglas G, et al. JCAD, a Gene at the 10p11 Coronary Artery Disease Locus, Regulates Hippo Signaling in Endothelial Cells. Arterioscler Thromb Vasc Biol. 2018;38:1711-22.
[83] Oh DS, Lee HK. Autophagy protein ATG5 regulates CD36 expression and anti-tumor MHC class II antigen presentation in dendritic cells. Autophagy. 2019;15:2091-106.
[84] Maxwell CA, Keats JJ, Crainie M, Sun X, Yen T, Shibuya E, et al. RHAMM is a centrosomal protein that interacts with dynein and maintains spindle pole stability. Mol Biol Cell. 2003;14:2262-76.
[85] Rolseth V, Krokeide SZ, Kunke D, Neurauter CG, Suganthan R, Sejersted Y, et al. Loss of Neil3, the major DNA glycosylase activity for removal of hydantoins in single stranded DNA, reduces cellular proliferation and sensitizes cells to genotoxic stress. Biochim Biophys Acta. 2013;1833:1157-64.

[86] Pan YQ, Hou AN. Hyperoxia-induced lung injury increases CDKN1A levels in a newborn rat model of bronchopulmonary dysplasia. Exp Lung Res. 2018;44:424-32.
[87] McGrath-Morrow SA, Cho C, Soutiere S, Mitzner W, Tuder R. The effect of neonatal hyperoxia on the lung of p21Waf1/Cip1/Sdi1-deficient mice. Am J Respir Cell Mol Biol. 2004;30:635-40.
[88] de Vries M, Faiz A, Woldhuis RR, Postma DS, de Jong TV, Sin DD, et al. Lung tissue gene-expression signature for the ageing lung in COPD. Thorax. 2017.
[89] Hellborg F, Qian W, Mendez-Vidal C, Asker C, Kost-Alimova M, Wilhelm M, et al. Human wig-1, a p53 target gene that encodes a growth inhibitory zinc finger protein. Oncogene. 2001;20:5466-74.
[90] Leszczynska KB, Foskolou IP, Abraham AG, Anbalagan S, Tellier C, Haider S, et al. Hypoxia-induced p53 modulates both apoptosis and radiosensitivity via AKT. J Clin Invest. 2015;125:2385-98.
[91] Pendeville H, Winandy M, Manfroid I, Nivelles O, Motte P, Pasque V, et al. Zebrafish Sox7 and Sox18 function together to control arterial-venous identity. Dev Biol. 2008;317:405-16.
[92] Costa G, Mazan A, Gandillet A, Pearson S, Lacaud G, Kouskoff V. SOX7 regulates the expression of VE-cadherin in the haemogenic endothelium at the onset of haematopoietic development. Development. 2012;139:1587-98.
[93] Xu Y, An X, Guo X, Habtetsion TG, Wang Y, Xu X, et al. Endothelial PFKFB3 plays a critical role in angiogenesis. Arterioscler Thromb Vasc Biol. 2014;34:1231-9.
[94] Takahashi D, Mori T, Wakabayashi M, Mori Y, Susa K, Zeniya M, et al. KLHL2 interacts with and ubiquitinates WNK kinases. Biochem Biophys Res Commun. 2013;437:457-62.
[95] Jiang H, Huang S, Li X, Li X, Zhang Y, Chen ZY. Tyrosine kinase receptor B protects against coronary artery disease and promotes adult vasculature integrity by regulating Ets1-mediated VE-cadherin expression. Arterioscler Thromb Vasc Biol. 2015;35:580-8.
[96] Kermani P, Rafii D, Jin DK, Whitlock P, Schaffer W, Chiang A, et al. Neurotrophins promote revascularization by local recruitment of TrkB+ endothelial cells and systemic mobilization of hematopoietic progenitors. J Clin Invest. 2005;115:653-63.
[97] Matsuda S, Fujita T, Kajiya M, Takeda K, Shiba H, Kawaguchi H, et al. Brain-derived neurotrophic factor induces migration of endothelial cells through a TrkB-ERK-integrin alphaVbeta3-FAK cascade. J Cell Physiol. 2012;227:2123-9.
[98] Totoson P, Pedard M, Marie C, Demougeot C. Activation of endothelial TrkB receptors induces relaxation of resistance arteries. Vascul Pharmacol. 2018;106:46-53.
[99] Eelen G, Dubois C, Cantelmo AR, Goveia J, Bruning U, DeRan M, et al. Role of glutamine synthetase in angiogenesis beyond glutamine synthesis. Nature. 2018;561:63-9.
[100] McAlhany SJ, Ressler SJ, Larsen M, Tuxhorn JA, Yang F, Dang TD, et al. Promotion of angiogenesis by ps20 in the differential reactive stroma prostate cancer xenograft model. Cancer Res. 2003;63:5859-65.
[101] Johnson LA, Banerji S, Lawrance W, Gileadi U, Prota G, Holder KA, et al. Dendritic cells enter lymph vessels by hyaluronan-mediated docking to the endothelial receptor LYVE-1. Nat Immunol. 2017;18:762-70.
[102] Choi BH, Suzuki M, Kim T, Wagner SL, Cunningham DD. Protease nexin-1. Localization in the human brain suggests a protective role against extravasated serine proteases. Am J Pathol. 1990;137:741-7.
[103] Wang X, Wei X, Yuan Y, Sun Q, Zhan J, Zhang J, et al. Src-mediated phosphorylation converts FHL1 from tumor suppressor to tumor promoter. J Cell Biol. 2018;217:1335-51.

[104] Razani B, Wang XB, Engelman JA, Battista M, Lagaud G, Zhang XL, et al. Caveolin-2-deficient mice show evidence of severe pulmonary dysfunction without disruption of caveolae. Mol Cell Biol. 2002;22:2329-44.
[105] Abdelsaid MA, Matragoon S, Ergul A, El-Remessy AB. Deletion of thioredoxin interacting protein (TXNIP) augments hyperoxia-induced vaso-obliteration in a mouse model of oxygen induced-retinopathy. PLoS One. 2014;9:e110388.
[106] Ou X, O'Leary HA, Broxmeyer HE. Implications of DPP4 modification of proteins that regulate stem/progenitor and more mature cell types. Blood. 2013;122:161-9.
[107] Zhu B, Zhang L, Creighton J, Alexeyev M, Strada SJ, Stevens T. Protein kinase A phosphorylation of tau-serine 214 reorganizes microtubules and disrupts the endothelial cell barrier. Am J Physiol Lung Cell Mol Physiol. 2010;299:L493-501.
[108] Tugues S, Honjo S, Konig C, Padhan N, Kroon J, Gualandi L, et al. Tetraspanin CD63 promotes vascular endothelial growth factor receptor 2-beta1 integrin complex formation, thereby regulating activation and downstream signaling in endothelial cells in vitro and in vivo. J Biol Chem. 2013;288:19060-71.
[109] Liu J, Zhang Z, Chai L, Che Y, Min S, Yang R. Identification and characterization of a unique leucine-rich repeat protein (LRRC33) that inhibits Toll-like receptor-mediated NF-kappaB activation. Biochem Biophys Res Commun. 2013;434:28-34.
[110] Wang Y, Tong X, Omoregie ES, Liu W, Meng S, Ye X. Tetraspanin 6 (TSPAN6) negatively regulates retinoic acid-inducible gene I-like receptor-mediated immune signaling in a ubiquitination-dependent manner. J Biol Chem. 2012;287:34626-34.
[111] Iosef C, Alastalo TP, Hou Y, Chen C, Adams ES, Lyu SC, et al. Inhibiting NF-kappaB in the developing lung disrupts angiogenesis and alveolarization. Am J Physiol Lung Cell Mol Physiol. 2012;302:L1023-36.
[112] Samitas K, Poulos N, Semitekolou M, Morianos I, Tousa S, Economidou E, et al. Activin-A is overexpressed in severe asthma and is implicated in angiogenic processes. Eur Respir J. 2016;47:769-82.
[113] George EL, Georges-Labouesse EN, Patel-King RS, Rayburn H, Hynes RO. Defects in mesoderm, neural tube and vascular development in mouse embryos lacking fibronectin. Development. 1993;119:1079-91.
[114] Jo DY, Rafii S, Hamada T, Moore MA. Chemotaxis of primitive hematopoietic cells in response to stromal cell-derived factor-1. J Clin Invest. 2000;105:101-11.
[115] Gillich A, Zhang F, Farmer CG, Travaglini KJ, Tan SY, Gu M, et al. Capillary cell-type specialization in the alveolus. Nature. 2020;586:785-9.
[116] Malinverno M, Corada M, Ferrarini L, Formicola L, Marazzi G, Sassoon D, et al. Peg3/PW1 Is a Marker of a Subset of Vessel Associated Endothelial Progenitors. Stem Cells. 2017;35:1328-40.
[117] Relaix F, Wei XJ, Wu X, Sassoon DA. Peg3/Pw1 is an imprinted gene involved in the TNF-NFkappaB signal transduction pathway. Nat Genet. 1998;18:287-91.
[118] Iosef C, Liu M, Ying L, Rao SP, Concepcion KR, Chan WK, et al. Distinct roles for IkappaB kinases alpha and beta in regulating pulmonary endothelial angiogenic function during late lung development. J Cell Mol Med. 2018;22:4410-22.
[119] Mahgoub L, Kaddoura T, Kameny AR, Lopez Ortego P, Vanderlaan RD, Kakadekar A, et al. Pulmonary vein stenosis of ex-premature infants with pulmonary hypertension and bronchopulmonary dysplasia, epidemiology, and survival from a multicenter cohort. Pediatric pulmonology. 2017;52:1063-70.

[120] Mai J, Virtue A, Shen J, Wang H, Yang XF. An evolving new paradigm: endothelial cells--conditional innate immune cells. J Hematol Oncol. 2013;6:61.
[121] Lingappan K, Jiang W, Wang L, Moorthy B. Sex-specific differences in neonatal hyperoxic lung injury. Am J Physiol Lung Cell Mol Physiol. 2016;311:L481-93.
[122] Wolterink-Donselaar IG, Meerding JM, Fernandes C. A method for gender determination in newborn dark pigmented mice. Lab Anim (NY). 2009;38:35-8.
[123] Hilgendorff A, Reiss I, Ehrhardt H, Eickelberg O, Alvira CM. Chronic Lung Disease in the Preterm Infant: Lessons Learned From Animal Models. Am J Respir Cell Mol Biol. 2013.
[124] Zanini F, Robinson ML, Croote D, Sahoo MK, Sanz AM, Ortiz-Lasso E, et al. Virus-inclusive single-cell RNA sequencing reveals the molecular signature of progression to severe dengue. Proc Natl Acad Sci U S A. 2018;115:E12363-E9.
[125] Picelli S, Bjorklund AK, Faridani OR, Sagasser S, Winberg G, Sandberg R. Smart-seq2 for sensitive full-length transcriptome profiling in single cells. Nat Methods. 2013;10:1096-8.
[126] Dobin A, Davis CA, Schlesinger F, Drenkow J, Zaleski C, Jha S, et al. STAR: ultrafast universal RNA-seq aligner. Bioinformatics. 2013;29:15-21.
[127] Anders S, Pyl PT, Huber W. HTSeq--a Python framework to work with high-throughput sequencing data. Bioinformatics. 2015;31:166-9.
[128] Koster J, Rahmann S. Snakemake--a scalable bioinformatics workflow engine. Bioinformatics. 2012;28:2520-2.
[129] Pedregosa F, Varoquaux G, Gramfort A, Michel V, Thirion B, Grisel O, et al. Scikit-learn: Machine Learning in Python. J Mach Learn Res. 2011;12:2825-30.
[130] Traag VA, Waltman L, van Eck NJ. From Louvain to Leiden: guaranteeing well-connected communities. Sci Rep. 2019;9:5233.
[131] Zhou Y, Zhou B, Pache L, Chang M, Khodabakhshi AH, Tanaseichuk O, et al. Metascape provides a biologist-oriented resource for the analysis of systems-level datasets. Nat Commun. 2019;10:1523.
[132] Clifford PS, Ella SR, Stupica AJ, Nourian Z, Li M, Martinez-Lemus LA, et al. Spatial distribution and mechanical function of elastin in resistance arteries: a role in bearing longitudinal stress. Arterioscler Thromb Vasc Biol. 2011;31:2889-96.

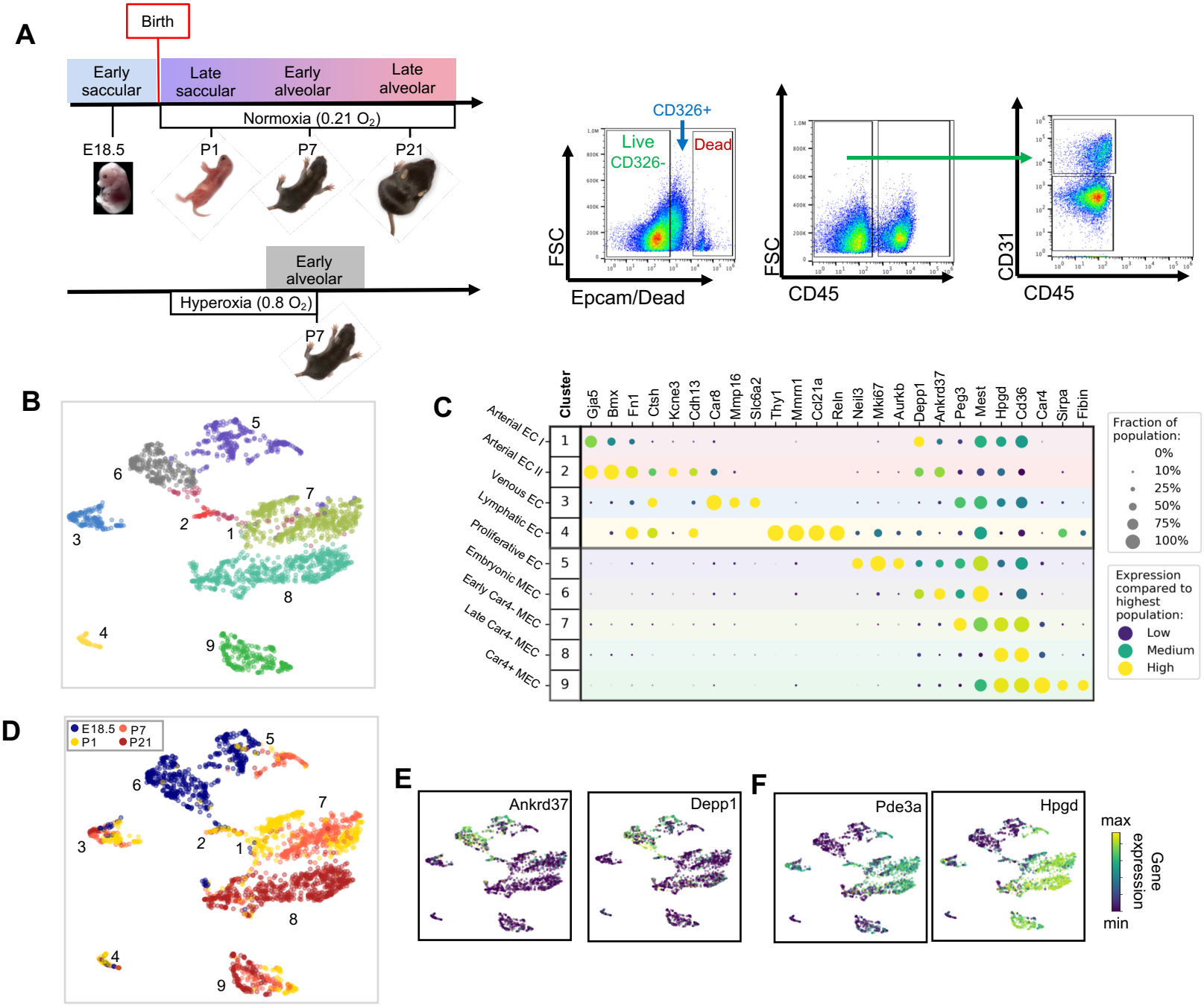
A
Birth
Early saccular
Late saccular
Early alveolar
Late alveolar
Normoxia (0.21 O2)
E18.5
P1
P7
P21
Early alveolar
Hyperoxia (0.8 O2)
P7
CD326+
Live CD326-
Dead
FSC
Epcam/Dead
FSC
CD45
CD31
CD45
B
C
Cluster
Gja5
Bmx
Fn1
Ctsh
Kcne3
Cdh13
Car8
Mmp16
Slc6a2
Thy1
Mmrn1
Ccl21a
Reln
Neil3
Mki67
Aurkb
Depp1
Ankrd37
Peg3
Mest
Hpgd
Cd36
Car4
Sirpa
Fibin
Arterial EC I
Arterial EC II
Venous EC
Lymphatic EC
Proliferative EC
Embryonic MEC
Early Car4- MEC
Late Car4- MEC
Car4+ MEC
Fraction of population:
0%
10%
25%
50%
75%
100%
Expression compared to highest population:
Low
Medium
High
D
E18.5
P1
P7
P21
E
Ankrd37
Depp1
F
Pde3a
Hpgd
max
min
Gene expression

Figure 1

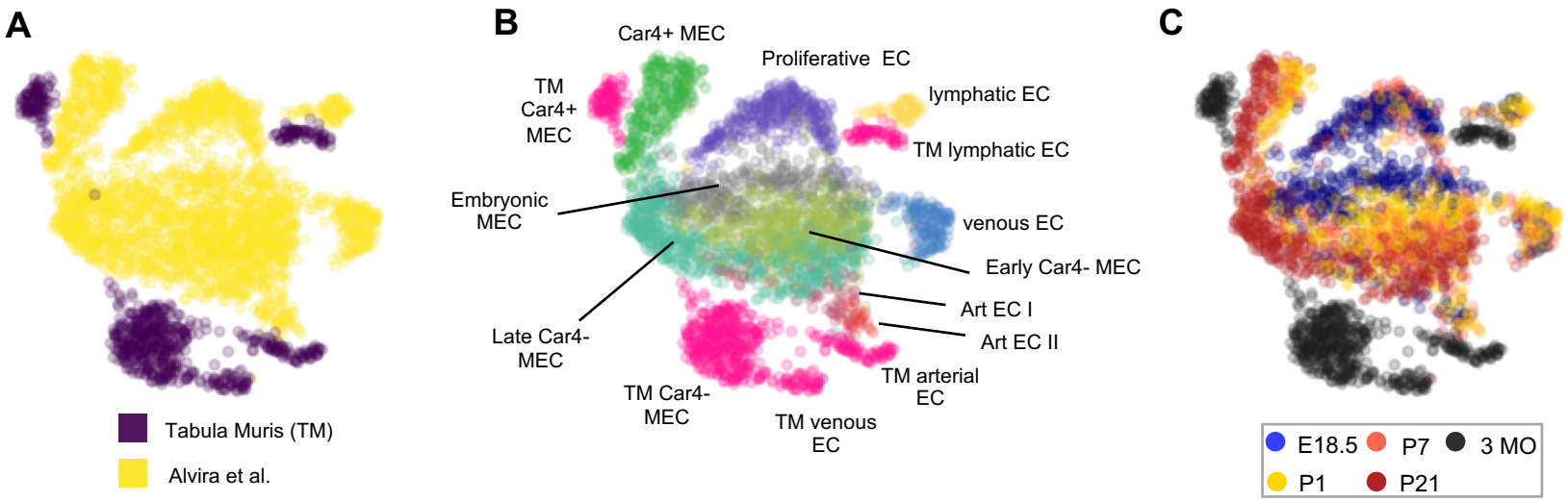
A
Tabula Muris (TM)
Alvira et al.
B
Car4+ MEC
Proliferative EC
TM Car4+ MEC
lymphatic EC
TM lymphatic EC
Embryonic MEC
venous EC
Early Car4- MEC
Art EC I
Art EC II
Late Car4- MEC
TM arterial EC
TM Car4- MEC
TM venous EC
C
E18.5
P7
3 MO
P1
P21

Figure 2

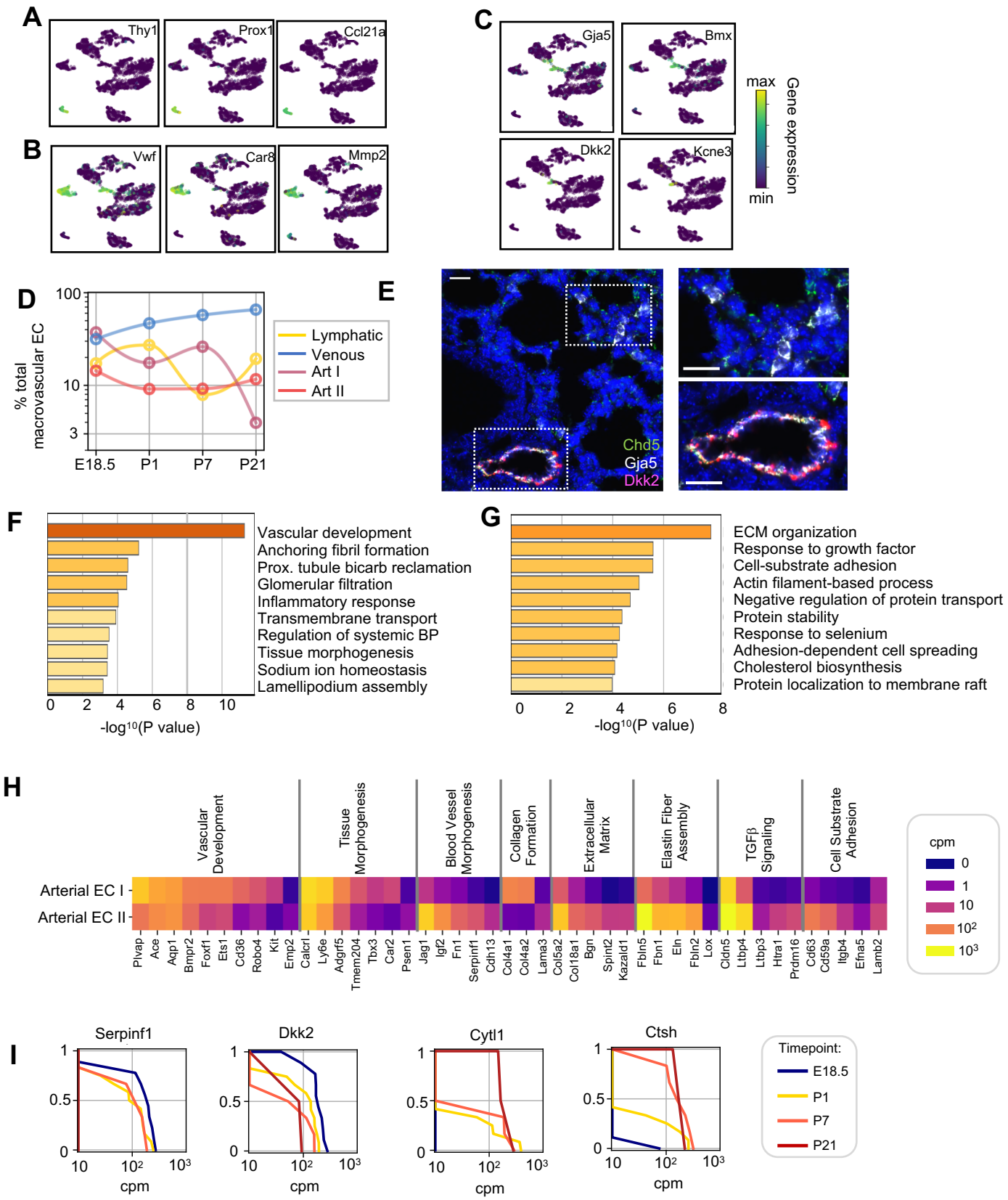
A
Thy1
Prox1
Ccl21a
B
Vwf
Car8
Mmp2
C
Gja5
Bmx
Dkk2
Kcne3
max
min
Gene expression
D
% total macrovascular EC
100
10
3
E18.5
P1
P7
P21
Lymphatic
Venous
Art I
Art II
E
Chd5
Gja5
Dkk2
F
Vascular development
Anchoring fibril formation
Prox. tubule bicarb reclamation
Glomerular filtration
Inflammatory response
Transmembrane transport
Regulation of systemic BP
Tissue morphogenesis
Sodium ion homeostasis
Lamellipodium assembly
0 2 4 6 8 10
-log10(P value)
G
ECM organization
Response to growth factor
Cell-substrate adhesion
Actin filament-based process
Negative regulation of protein transport
Protein stability
Response to selenium
Adhesion-dependent cell spreading
Cholesterol biosynthesis
Protein localization to membrane raft
0 2 4 6 8
-log10(P value)
H
Vascular Development
Tissue Morphogenesis
Blood Vessel Morphogenesis
Collagen Formation
Extracellular Matrix
Elastin Fiber Assembly
TGFβ Signaling
Cell Substrate Adhesion
Arterial EC I
Arterial EC II
Plvap Ace Aqp1 Bmpr2 Foxf1 Ets1 Cd36 Robo4 Kit Emp2 Calcrl Ly6e Adgrf5 Tmem204 Tbx3 Car2 Psen1 Jag1 Igf2 Fn1 Serpinf1 Cdh13 Col4a1 Col4a2 Lama3 Col5a2 Col18a1 Bgn Spint2 Kazald1 Fbln5 Fbn1 Eln Fbln2 Lox Cldn5 Ltbp4 Ltbp3 Htra1 Prdm16 Cd63 Cd59a Itgb4 Efna5 Lamb2
cpm
0
1
10
10²
10³
I
Serpinf1
Dkk2
Cytl1
Ctsh
1
0.5
0
10
10²
10³
cpm
Timepoint:
E18.5
P1
P7
P21

Figure 3

Figure 4

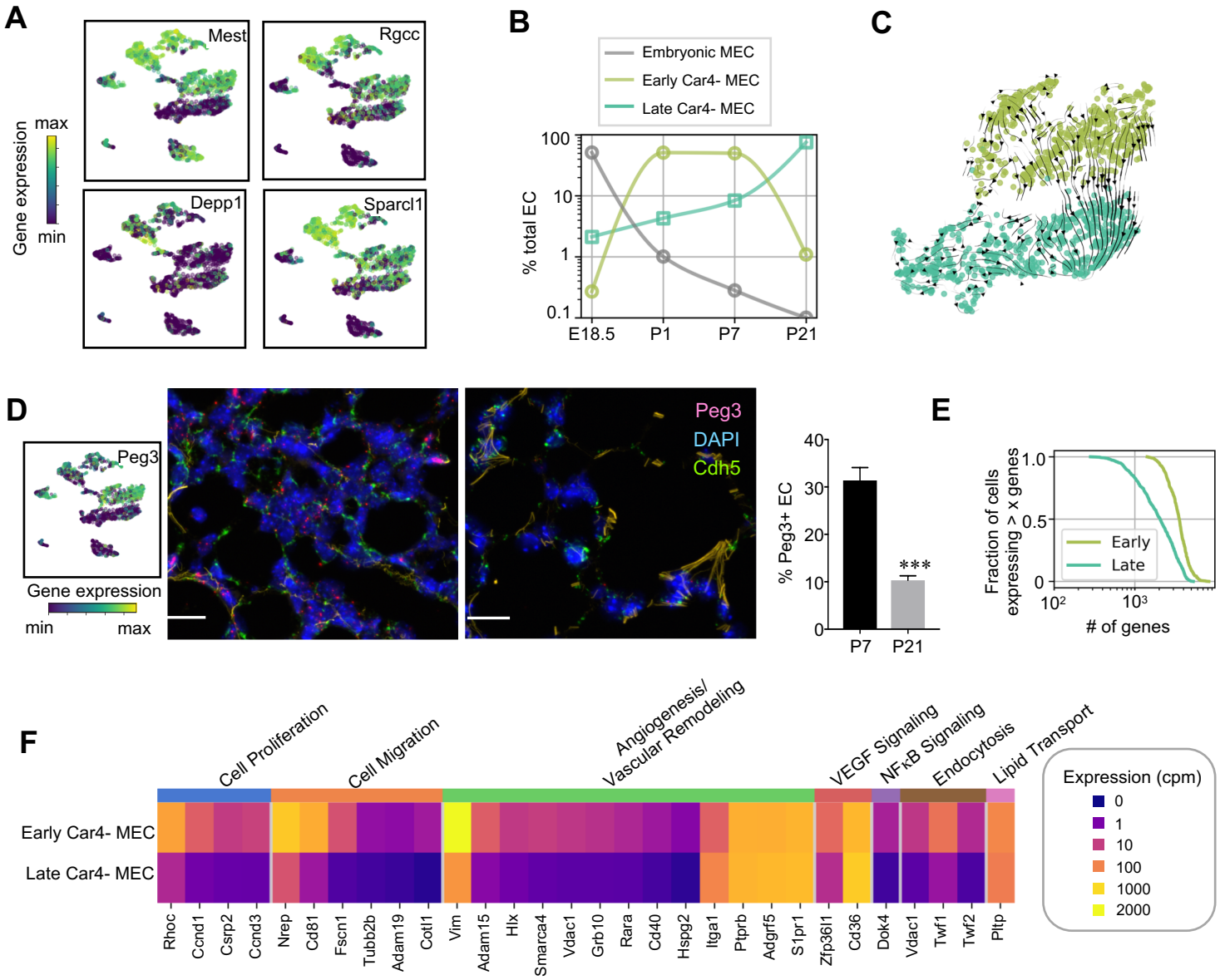
A
Mest
Rgcc
Depp1
Sparcl1
Gene expression
max
min
B
Embryonic MEC
Early Car4- MEC
Late Car4- MEC
% total EC
100
10
1
0.1
E18.5
P1
P7
P21
C
D
Peg3
Gene expression
min
max
Peg3
DAPI
Cdh5
% Peg3+ EC
40
30
20
10
0
***
P7
P21
E
Fraction of cells expressing > x genes
1.0
0.5
0
Early
Late
10^2
10^3
# of genes
F
Cell Proliferation
Cell Migration
Angiogenesis/ Vascular Remodeling
VEGF Signaling
NFκB Signaling
Endocytosis
Lipid Transport
Early Car4- MEC
Late Car4- MEC
Rhoc
Ccnd1
Csrp2
Ccnd3
Nrep
Cd81
Fscn1
Tubb2b
Adam19
Cotl1
Vim
Adam15
Hlx
Smarca4
Vdac1
Grb10
Rara
Cd40
Hspg2
Itga1
Ptprb
Adgrf5
S1pr1
Zfp36l1
Cd36
Dok4
Vdac1
Twf1
Twf2
Pltp
Expression (cpm)
0
1
10
100
1000
2000

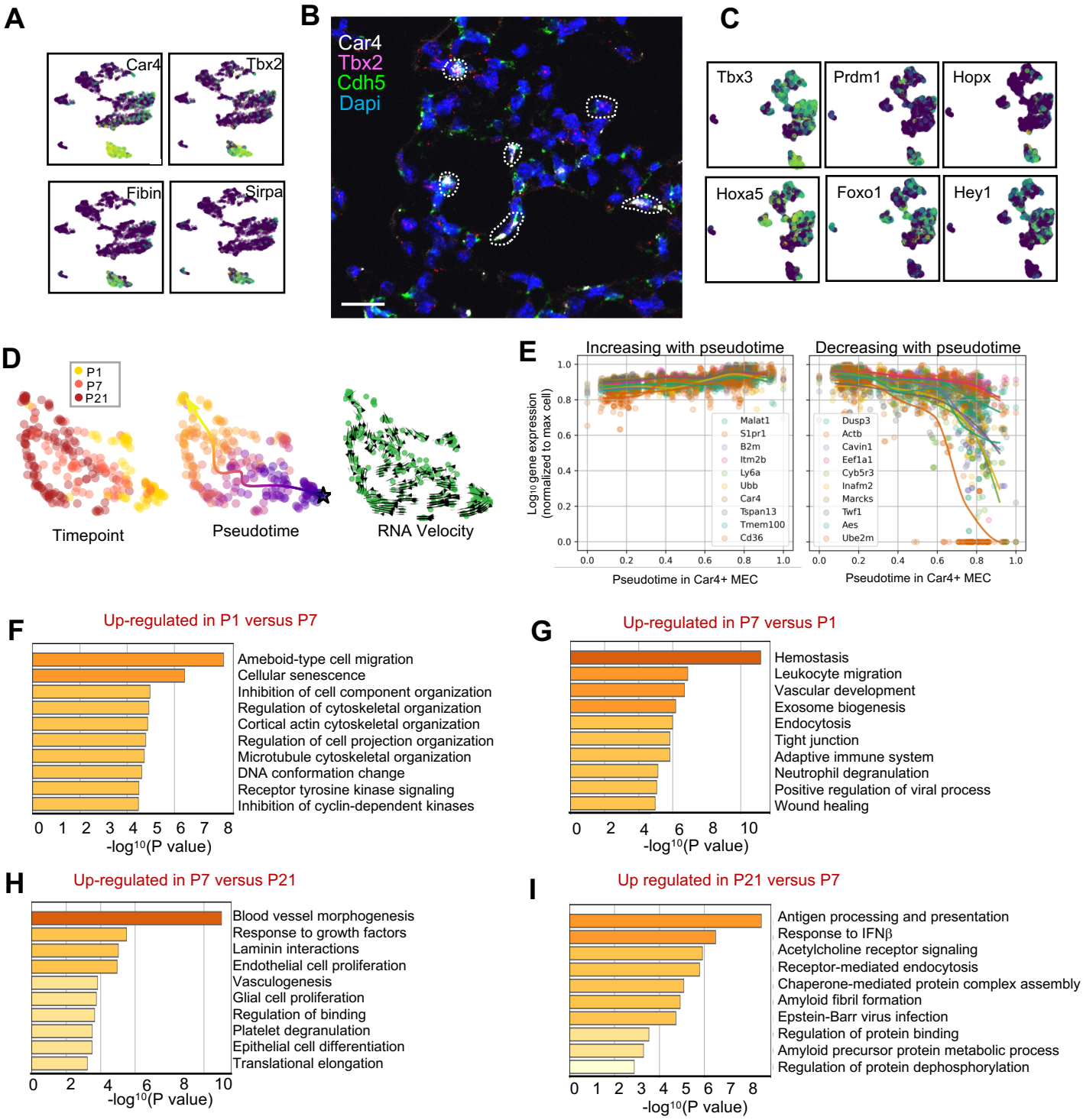
A
Car4
Tbx2
Fibin
Sirpa
B
Car4
Tbx2
Cdh5
Dapi
C
Tbx3
Prdm1
Hopx
Hoxa5
Foxo1
Hey1
D
P1
P7
P21
Timepoint
Pseudotime
RNA Velocity
E
Increasing with pseudotime
Decreasing with pseudotime
Log10 gene expression (normalized to max cell)
Malat1
S1pr1
B2m
Itm2b
Ly6a
Ubb
Car4
Tspan13
Tmem100
Cd36
Dusp3
Actb
Cavin1
Eef1a1
Cyb5r3
Inafm2
Marcks
Twf1
Aes
Ube2m
Pseudotime in Car4+ MEC
Pseudotime in Car4+ MEC
F
Up-regulated in P1 versus P7
Ameboid-type cell migration
Cellular senescence
Inhibition of cell component organization
Regulation of cytoskeletal organization
Cortical actin cytoskeletal organization
Regulation of cell projection organization
Microtubule cytoskeletal organization
DNA conformation change
Receptor tyrosine kinase signaling
Inhibition of cyclin-dependent kinases
-log10(P value)
G
Up-regulated in P7 versus P1
Hemostasis
Leukocyte migration
Vascular development
Exosome biogenesis
Endocytosis
Tight junction
Adaptive immune system
Neutrophil degranulation
Positive regulation of viral process
Wound healing
-log10(P value)
H
Up-regulated in P7 versus P21
Blood vessel morphogenesis
Response to growth factors
Laminin interactions
Endothelial cell proliferation
Vasculogenesis
Glial cell proliferation
Regulation of binding
Platelet degranulation
Epithelial cell differentiation
Translational elongation
-log10(P value)
I
Up regulated in P21 versus P7
Antigen processing and presentation
Response to IFNβ
Acetylcholine receptor signaling
Receptor-mediated endocytosis
Chaperone-mediated protein complex assembly
Amyloid fibril formation
Epstein-Barr virus infection
Regulation of protein binding
Amyloid precursor protein metabolic process
Regulation of protein dephosphorylation
-log10(P value)
J
Cell Migration
Cytoskeletal Organization
Vascular Development
Blood Vessel Morphogenesis
Laminin Interactions
Antigen Presentation
Pseudotime
Relative expression
High
Mid
Low
None
Itga4
Itga2
Sparc
Adam10
Fgf1
Mark4
Tmsb10
Rock2
Actb
Fmnl2
Ecm1
Eng
Tspan12
Cav2
Ywhaz
Calcrl
Ctnnb1
Ahr
Id1
Sox18
Jcad
Egf17
Adam12
Hapln1
Nid2
Fscn1
Nid1
H2-D1
H2-K1
Clu
Cd36

Figure 5

Figure 6

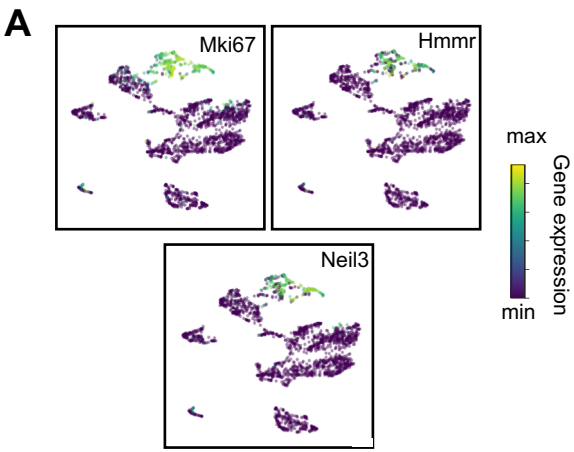

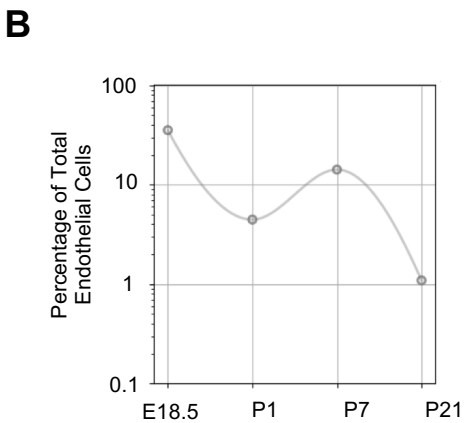

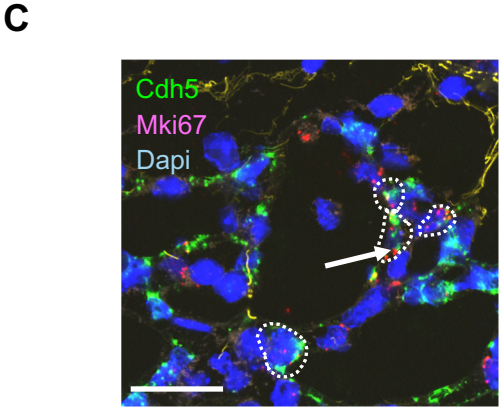

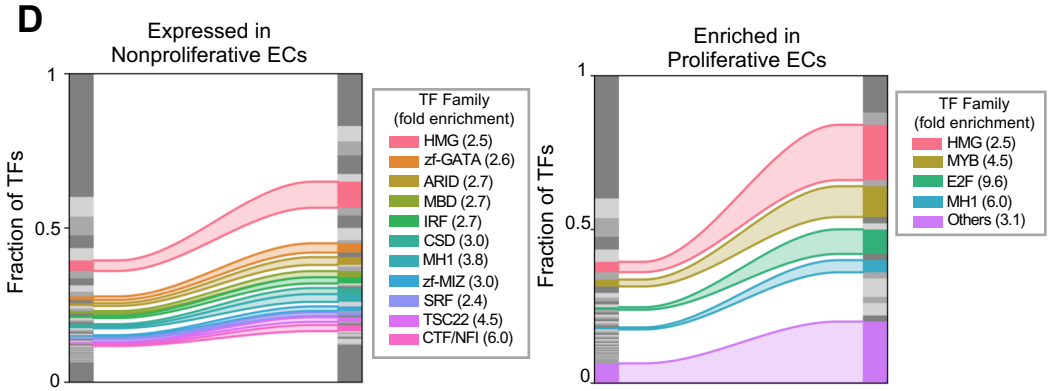

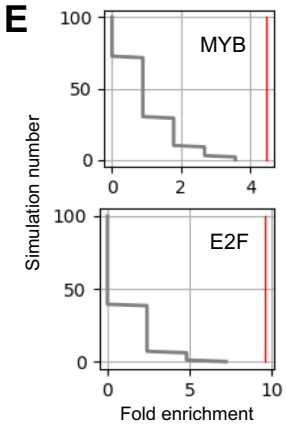

F

Gene	log2 fold change	P value
Mybl2	1.91	0.00952
Tfdp1	1.76	0.00001
Mier3	1.45	0.02793
E2f2	0.94	0.04292
Zzz3	0.88	0.00336
Mybl1	0.56	0.00183
Smarcc2	-0.94	0.02965
Terf1	-1.01	0.00921

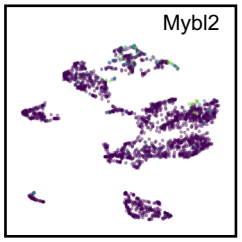

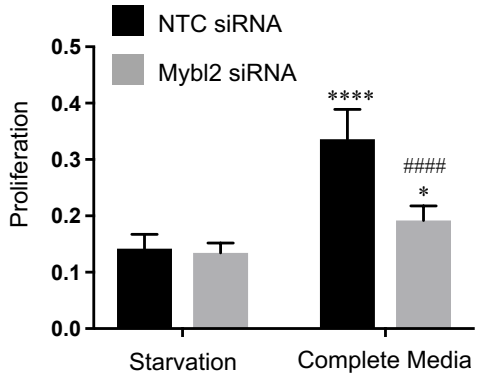

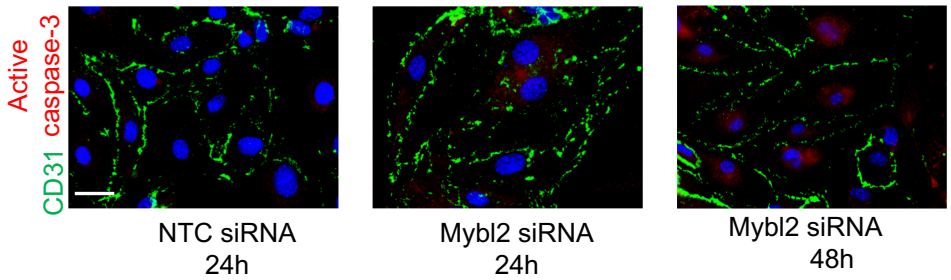

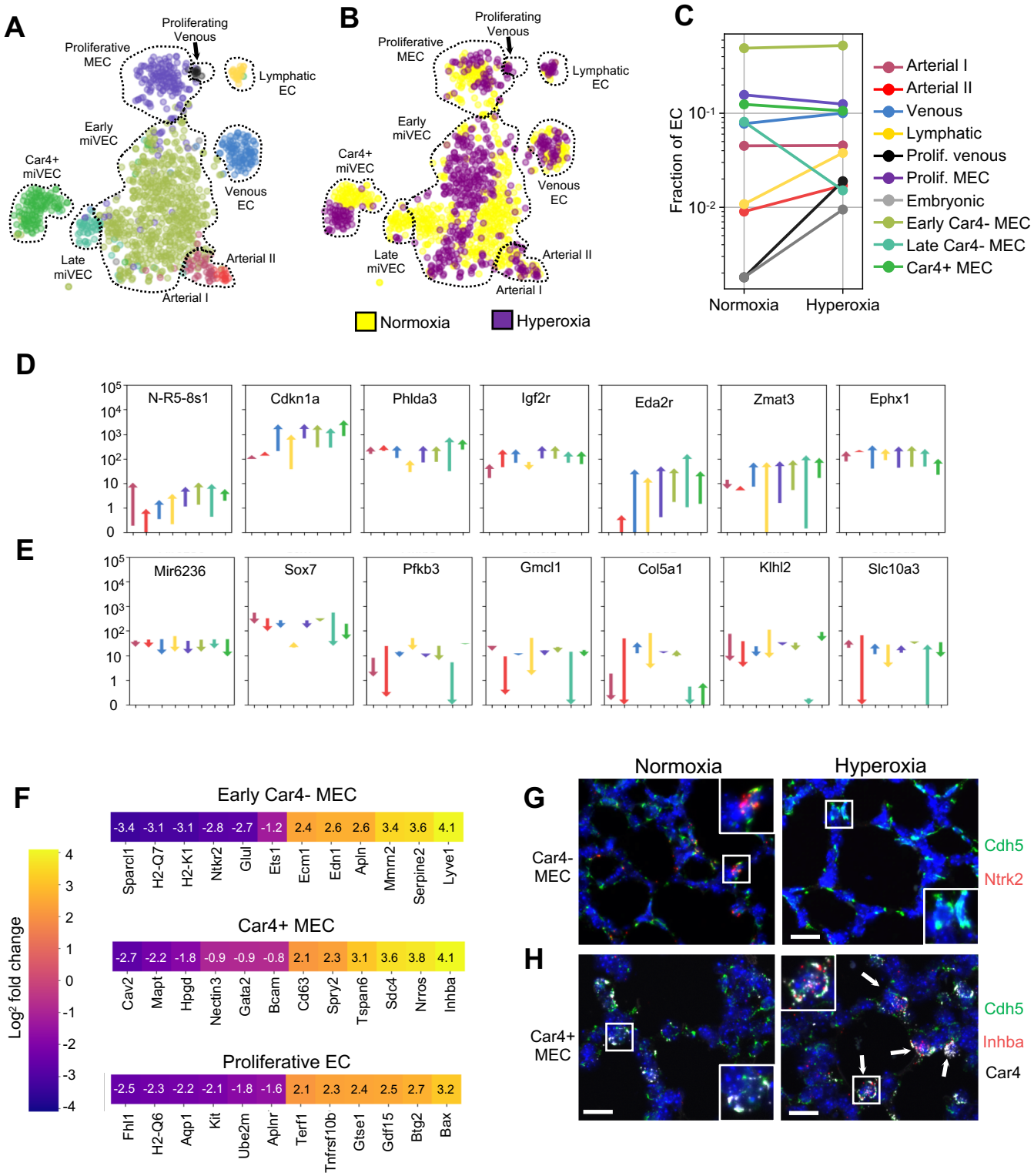
A
Proliferating Venous
Proliferative MEC
Lymphatic EC
Early miVEC
Car4+ miVEC
Venous EC
Late miVEC
Arterial II
Arterial I
B
Proliferating Venous
Proliferative MEC
Lymphatic EC
Early miVEC
Car4+ miVEC
Venous EC
Late miVEC
Arterial II
Arterial I
Normoxia
Hyperoxia
C
Fraction of EC
Normoxia
Hyperoxia
Arterial I
Arterial II
Venous
Lymphatic
Prolif. venous
Prolif. MEC
Embryonic
Early Car4- MEC
Late Car4- MEC
Car4+ MEC
D
N-R5-8s1
Cdkn1a
Phlda3
Igf2r
Eda2r
Zmat3
Ephx1
E
Mir6236
Sox7
Pfkb3
Gmcl1
Col5a1
Klhl2
Slc10a3
F
Early Car4- MEC
-3.4 -3.1 -3.1 -2.8 -2.7 -1.2 2.4 2.6 2.6 3.4 3.6 4.1
Sparcl1 H2-Q7 H2-K1 Ntkr2 Glul Ets1 Ecm1 Edn1 Apln Mmrn2 Serpine2 Lyve1
Car4+ MEC
-2.7 -2.2 -1.8 -0.9 -0.9 -0.8 2.1 2.3 3.1 3.6 3.8 4.1
Cav2 Mapt Hpgd Nectin3 Gata2 Bcam Cd63 Spry2 Tspan6 Sdc4 Nrros Inhba
Proliferative EC
-2.5 -2.3 -2.2 -2.1 -1.8 -1.6 2.1 2.3 2.4 2.5 2.7 3.2
Fhl1 H2-Q6 Aqp1 Kit Ube2m Aplnr Terf1 Tnfrsf10b Gtse1 Gdf15 Btg2 Bax
Log2 fold change
G
Normoxia
Hyperoxia
Car4-MEC
Cdh5
Ntrk2
H
Car4+ MEC
Cdh5
Inhba
Car4

Figure 7

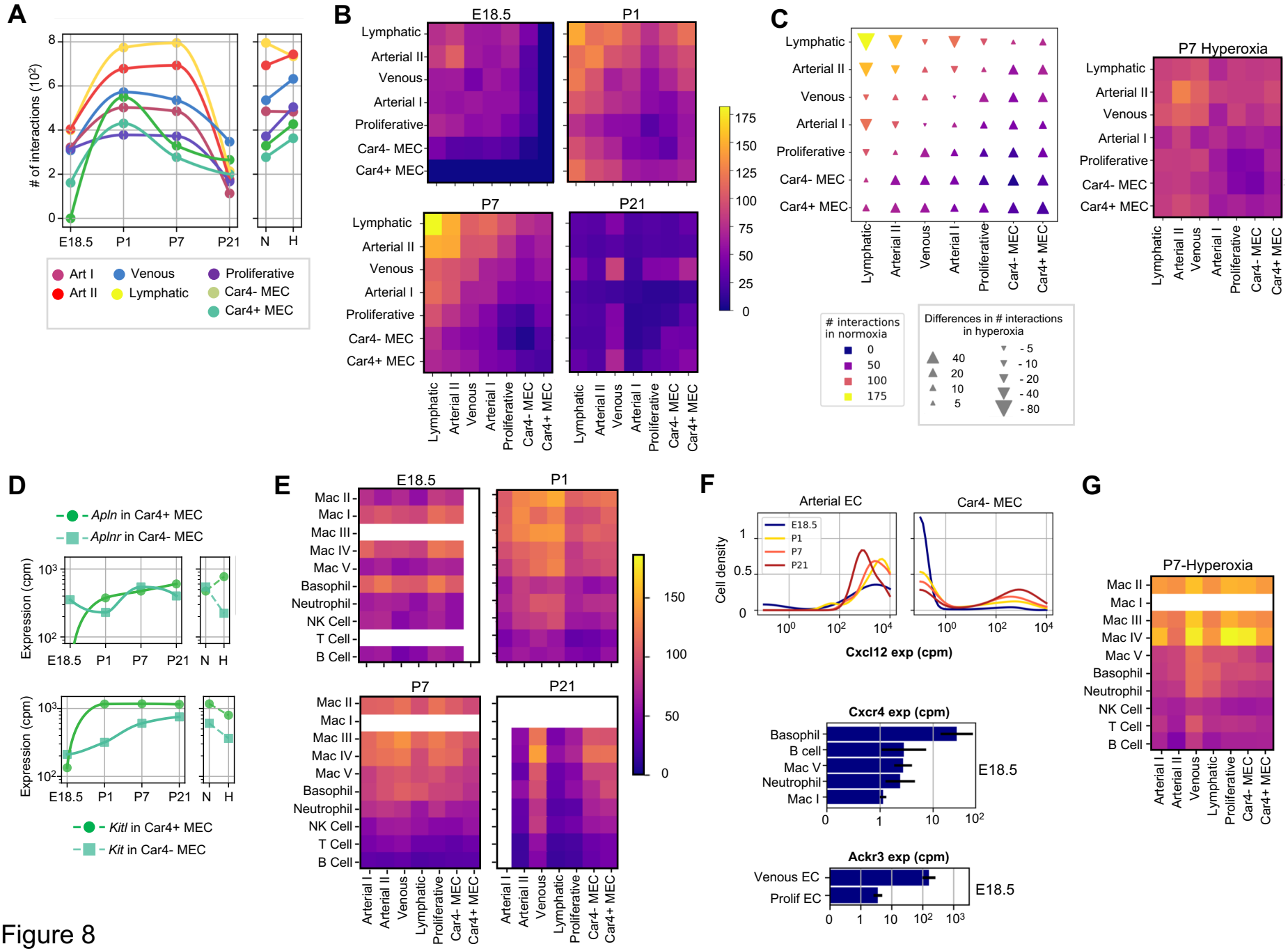
A
# of interactions (10²)
E18.5
P1
P7
P21
N
H
Art I
Art II
Venous
Lymphatic
Proliferative
Car4- MEC
Car4+ MEC
B
E18.5
P1
P7
P21
Lymphatic
Arterial II
Venous
Arterial I
Proliferative
Car4- MEC
Car4+ MEC
C
P7 Hyperoxia
interactions in normoxia
Differences in # interactions in hyperoxia
D
Apln in Car4+ MEC
Aplnr in Car4- MEC
Expression (cpm)
Kitl in Car4+ MEC
Kit in Car4- MEC
E
Mac II
Mac I
Mac III
Mac IV
Mac V
Basophil
Neutrophil
NK Cell
T Cell
B Cell
F
Arterial EC
Car4- MEC
Cell density
Cxcl12 exp (cpm)
Cxcr4 exp (cpm)
Ackr3 exp (cpm)
Venous EC
Prolif EC
G
P7-Hyperoxia

Figure 8

A

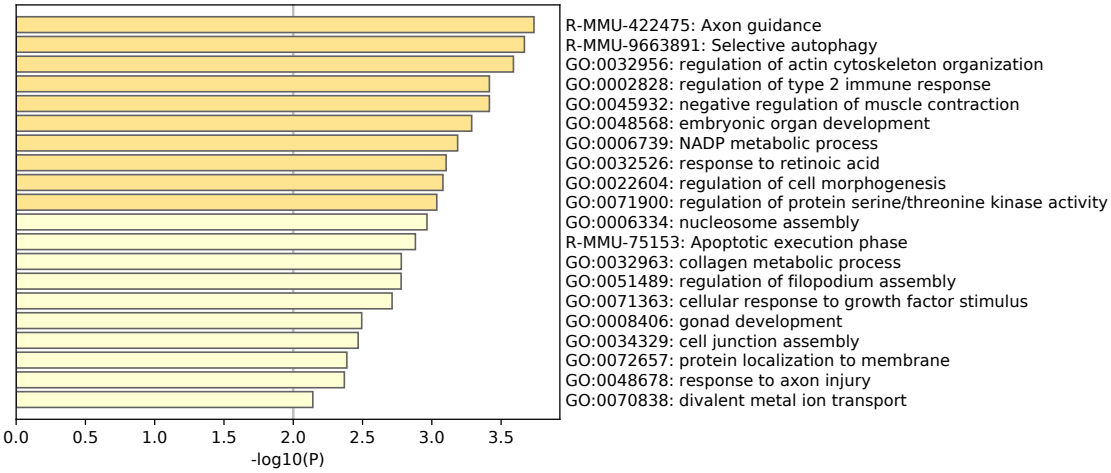

B

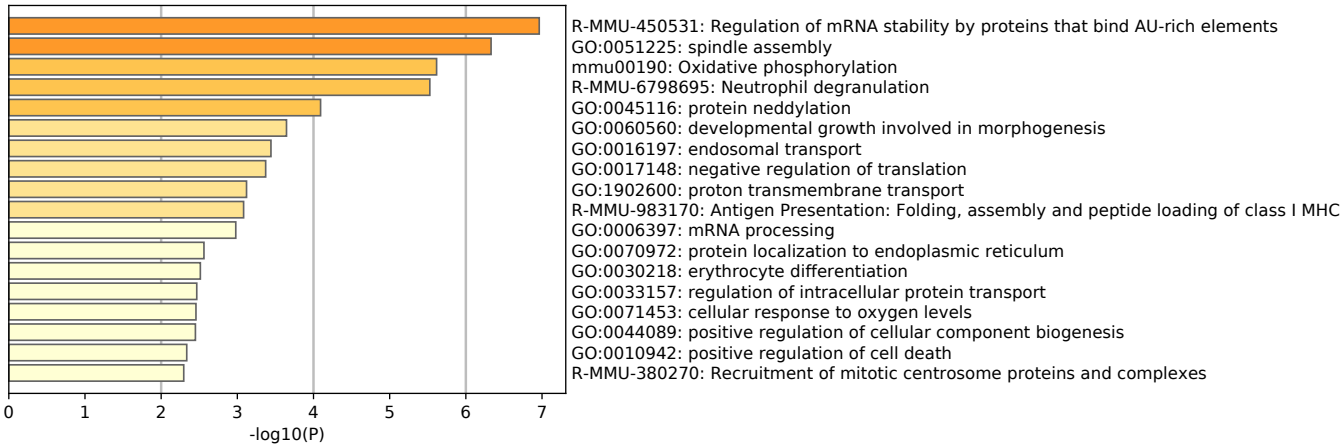

Supplemental Figure 1

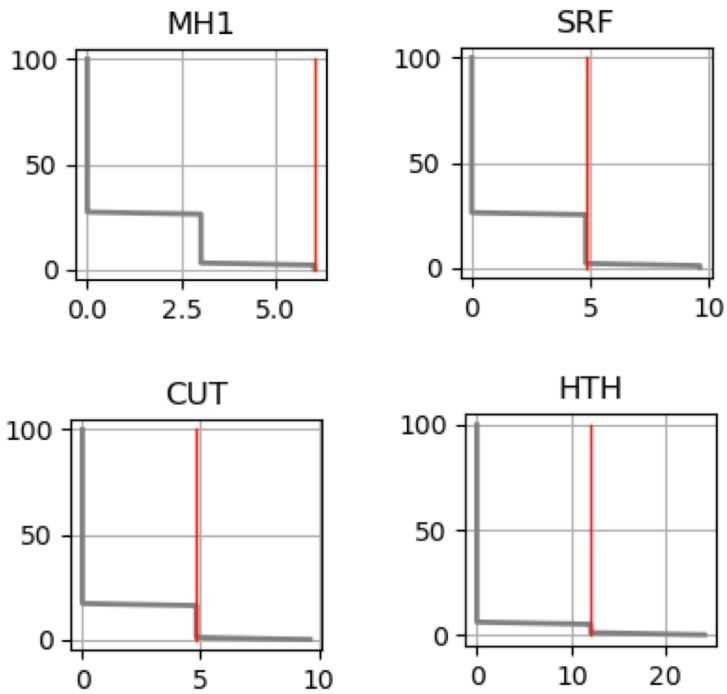

Supplemental Figure 2

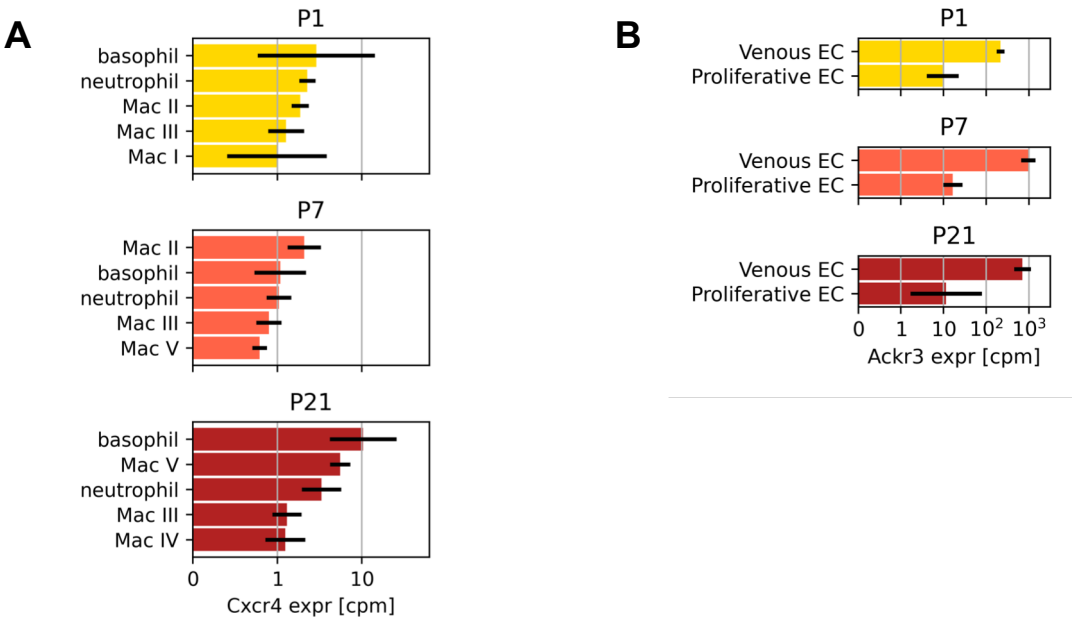

Supplemental Figure 3